Cement and Concrete Research 175 (2024) 107344

Contents lists available at ScienceDirect

Cement and Concrete Research

journal homepage: www.elsevier.com/locate/cemconres

A Bogue approach applied to basic oxygen furnace slag☆

J.C.O. Zepper [a,*], S.R. van der Laan [a,b], K. Schollbach [a], H.J.H. Brouwers [a]

[a] Department of the Built Environment, Eindhoven University of Technology, P. O. Box 513, 5600 MB Eindhoven, The Netherlands
[b] Tata Steel Netherlands, R&D, Microstructure & Surface Characterization (MSC), P.O. Box 10000, 1970CA IJmuiden, The Netherlands

ARTICLE INFO

Keywords:
Basic oxygen furnace slag
Modelling
Bogue approach
Quantitative XRD
Quantitative model assessment

ABSTRACT

Basic oxygen furnace (BOF) slag is an industrial by-product of the steel industry and has recently been investigated intensively for high-end applications other than road load and land fill. However, to be applied as a high-end raw material BOF slag lacks a quick and simple quantitative phase analysis method compared to the Bogue approach applied to ordinary Portland cement. This study presents a method to calculate the main phases of BOF slag (C_2S, $C_2(A,F)$, magnetite (Ff), RO-Phase and f-C) based on chemical composition. A quantitative model assessment was performed in order to further improve the model and two approaches were used to validate the Bogue BOF slag model. One approach compared the calculated chemical composition of phases with real data the second one evaluated whether the Bogue BOF slag model gives comparable quantitative model assessment measures compared to the classical cement Bogue approach. Both approaches validated the proposed final model.

1. Introduction

It has been almost 100 years ago since Bogue published his mathematical approach to quantify the phase composition of ordinary Portland cement (OPC) based on its chemical composition [1]. This approach became very popular in the cement and building industry and is still practiced today even though there have been technological advances such as quantitative X-ray diffraction analysis to quantify the clinker phases [2–4]. Knowledge of the phase proportions of OPCs is a necessity due to the fact that they control hydraulic properties and therefore strength [5,6], hence the knowledge can be used for quality control. The Rietveld quantitative phase analysis (RQPA) on X-ray diffraction patterns is a valuable, modern tool to determine the phase quantities of OPC. However, expert knowledge is required to accurately determine phase quantities due to the complexity of X-ray diffraction patterns of OPCs. The difficulty of RQPA applied to OPC has often been reported [4,7]. Therefore, the indirect determination of the phase proportions of OPCs by the usage of the Bogue equations remains an important tool in the cement industry and research.

It is recognized that the cement industry is causing a significant amount of the worlds CO_2 emissions (6–7 wt%) by producing OPCs. The main emissions (~90 wt%) are caused by fuel combustion and decomposition of $CaCO_3$ during the calcination process [8]. One way to reduce CO_2 emissions is by using industrial by-products as supplementary cementitious materials (SCMs) or by developing OPC free binders. One industrial by-product that has not been used much in such a way but has the potential for large scale application is basic oxygen furnace slag (BOF slag) or also known as Linz-Donawitz slag (LD slag) [9–11]. There are three major advantages: i) the large amount of BOF slag that is produced (>100 Mt/year worldwide) [12]; ii) the comparable chemical composition of BOF slag and OPCs with high CaO and SiO_2 concentration of >35 and >10 wt%, respectively [13]; iii) the comparable mineralogical composition of BOF slag to OPCs, since the major phases of BOF slag are C_2S and $C_2(A,F)$ [14,15]. Hence, BOF slag has been increasingly investigated for the application as SCM [10,16,17] or as a stand-alone binder through thermal [18], hydrothermal, chemical [9,19–22] and carbonation activation [23]. Table 1 presents the average and range of the chemical composition of BOF slag reported in the literature, while Table 2 presents the most common phases reported for BOF slag [10].

BOF slag is often inaccurately characterized in terms of phase composition by RQPA due to multiple reasons: i) the large number of phases (>5) and resulting peak overlap, ii) some phases may show preferred orientation (i.e. portlandite), iii) multiple polymorphs for some phases may be present (i.e. C_2S) [24], iv) impurities within phases may have effect on the powder pattern [4], v) solid solutions systems

☆ Dedicated to late Prof Dr. Herbert Pöllmann (1956 – 2022), Chairholder for Mineralogy andGeochemistry at the Martin-Luther University of Halle, Germany.

* Corresponding author.
E-mail address: j.c.o.zepper@tue.nl (J.C.O. Zepper).

https://doi.org/10.1016/j.cemconres.2023.107344
Received 17 February 2023; Received in revised form 27 September 2023; Accepted 7 October 2023
Available online 15 November 2023

exist [25,26] and vi) significant microabsorption effects when measuring samples containing more than >10 wt% Fe with Cu-radiation [27–29]. These reasons illustrate that an in-depth knowledge of the X-ray diffraction techniques and RQPA is required to accurately determine BOF slag phase composition and inaccurate results are easily obtained.

For this reason, this paper presents an alternative and simpler way to determine the BOF slag phase composition based on the Bogue approach. An equation sequence (i.e. Bogue BOF slag model) was derived that translates the chemical composition determined by X-ray fluorescence (XRF) and Fe-titration of BOF slag into phase quantities. For this purpose, BOF slag was sampled from processed batches, subsequently split, crushed and powdered so a representative sample was obtained. XRF, Fe-titration and RQPA were performed on powdered sampled material. Fe-titration is required to determine the redox state of the iron in the slag, as it can contain Fe(0), Fe(II) and Fe (III). The modelled phase quantities are then compared to the respective RQPA values and assessed quantitatively. The results were then used to improve the model and correct significant errors in the model. The corrected Bogue BOF slag model was applied to available literature data and discussed. Additionally, the performance of the corrected Bogue BOF slag model was compared to the classical cement Bogue model by using the same quantitative model assessment approach, which helped to evaluate its applicability.

2. Materials and methods

2.1. BOF slag sampling

The used BOF slag was produced at the Tata Steel steel plant IJmuiden, the Netherlands. The data set consists of 21 bulk samples from the BOF slag production referenced as “B” or “B-Type samples” that were sampled in the time period of 13.03 to 24.09.2020. Their size was between 0 and 25 mm. Each bulk sample represents approximately the average of weekly BOF slag production at the steel plant. The BOF slag samples were taken during a quality monitoring investigation from processed batches that contained multiple (>50) basic oxygen furnace heats (each 30 tons of BOF slag per heat) approximately every 9 days. The samples were taken according to standard NEN 7302:1999. The sampling method and its applicability to BOF slag sampling regarding the analysis by XRF, Fe redox titration and QXRD has been recently evaluated [30] and is reported in Table 3. Additionally, the chemical composition of five finer samples (0–1 mm) referenced as “F” or “F-Type

Table 2
Mineral name, formula and respective cement notation for the most common phases present in BOF slag.

Mineral name	Mineral formula	Cement notation
Larnite (Belite/β-C_2S), α -C_2S, α′-C_2S	Ca_2SiO_4	C_2S
Brownmillerite	$Ca_2(Fe,Al)_2O_5$	$C_2(A,F)$
Magnetite	Fe_3O_4	Ff
Periclase - Wuestite solid solution	(Mg,Fe,Mn)O	RO-Phase
Free Lime	CaO	f-C
Hatrurite (Alite)	Ca_3SiO_5	C_3S
Fe-Perovskite	$CaFe_2O_4$	CF
Calcite	$CaCO_3$	Cc
Portlandite	$Ca(OH)_2$	CH

Table 3
Global estimation errors (GE) for taking lot samples according to NEN 7302-1999 regarding XRF/Fe redox titration and QXRD, previously reported in [30].

Oxide	GE	Phase	GE
Al_2O_3	0.03	RO-Phase	0.50
CaO	0.15	Ff	0.68
Cr_2O_3	0.005	$C_2(A,F)$	0.68
Fe_2O_3	0.43	C_2S	0.41
FeO	0.41	C_3S	0.23
Met. Fe	0.18	f-C	0.09
MgO	0.09	CH	0.33
MnO	0.04	Cc	0.07
P_2O_5	0.010	Others	–
SiO_2	0.09	Amorphous	0.44
TiO_2	0.02		
V_2O_5	0.04		

Table 1
Chemical composition of BOF slag. Data has been derived from [10]. The references for the presented data can be found therein.

Year	CaO	Fe_{total} (Fe_2O_3/FeO/Fe)	SiO_2	Al_2O_3	MgO	MnO	$Na_2O + K_2O$
2020	40.82–54.29	16.78–29.49	8.45–16.93	0.33–5.85	1.93–9.15	1.2–8.7	0.27–0.84
2019	34.4–50.26	5.24–34.5	9.45–36.33	0.75–11.38	1.56–10.11	1.07–5.0	0.33–1.34
2018	34.21–46.8	18.01–29.56	10.8–20.38	1.01–7.46	2.7–9.95	0.42–5.17	0.13–0.41
2017	36.9–42.77	21.87–29.0	9.6–19.24	1.8–4.76	5.19–11.2	0.82–3.2	1.74–2.1
2016	33.97–49.92	20.49–37.6	8.58–26.1	1.12–6.8	2.0–9.5	2.4–10.31	0.02–0.24
2015	39.4–46.73	18.42–30.23	11.97–14.77	2.16–5.52	6.27–9.69	2.74–2.76	0.30
2014	35.5–40.95	10.88–30.2	12.2–32.08	4.76–7.73	6.57–8.55	1.26–3.97	–
2013	38.62–52.4	10.07–25.49	8.87–18.94	1.4–5.64	5.2–7.68	1.59–2.9	0.53
2012	40.1–57.44	17.47–32.0	8.6–15.84	1.7–4.86	4.5–8.41	1.77–3.7	0.10
2011	38.85–44.07	8.64–28.48	14.03–18.94	2.91–5.53	5.36–9.86	0.92–2.11	–
2010	40.46–47.71	23.86–24.36	13.25–17.09	3.04–4.53	6.37–10.46	2.64	0.42
Occurrence range	33.97–57.44	5.24–38.06	7.74–36.33	0.33–11.38	1.56–11.2	0.42–10.31	0.02–1.34
Mean values	42.17	23.80	14.77	3.53	6.80	3.02	0.31

Year	SO_3	Cr_2O_3	V_2O_5	TiO_2	P_2O_5	Other oxides
2020	0.07–0.71	0.14–0.33	0.42–0.53	0.16–1.57	0.89–7.14	1.07–1.3
2019	0.3–0.98	0.16–0.8	0.03–0.34	0.45–1.23	1.03–2.15	0.01–2.5
2018	0.01–0.3	0.7	0.1	0.45–0.68	1.12–2.78	1.73–1.98
2017	0.3	0.11	0.25	0.61	1.14	2.22
2016	0.12–2.7	0.21–1.2	6.51	0.25–1.78	0.81–2.32	–
2015	0.12	0.2	0.9	0.4–1.18	1.0–1.67	–
2014	0.18–0.74	3.14	–	0.32	0.25	3.11
2013	0.18–0.88	–	–	0.7	0.33–2.3	0.41–14.84
2012	0.4–1.2	–	–	0.5–0.81	1.4–2.4	–
2011	0.14–0.36	–	–	–	1.07	3.06–5.9
2010	–	–	–	0.67	1.47	–
Occurrence range	0.01–2.7	0.11–3.14	0.03–6.51	0.16–1.78	0.33–7.14	0.01–14.84
Mean values	0.47	0.63	0.90	0.78	1.76	2.95

Table 4
Stoichiometry and ICSD/PDF Nr. database codes used for the structures in the RQPA of BOF slag samples. It should be noted that a fixed stoichiometry is in all cases. The specific stoichiometry that is used for $C_2(A,F)$ is calculated from chemical compositions determined by large area phase mapping analysis (PARC) on average BOF slag samples from the Tata Steel plant IJmuinden [13].

Mineral name	Cement notation	Stoichiometry	ICSD/PDF-Nr.	Space group
Si-metallic standard	–	Si	43610/–	Fd-3m
Fe-rich Wuestite solid solution	RO	$Fe_{0.8}Mn_{0.2}O$	67200/–	Fm-3m
Mg-rich Wuestite solid solution	RO	$Fe_{0.3}Mg_{0.7}O$	67200/–	Fm-3m
Magnetite	Ff	Fe_3O_4	30860/–	Fd-3mZ
Brownmillerite	$C_2(A,F)$	$Ca_2Al_{0.79}Ti_{0.61}Fe_{1.59}O_5$	–/04-014-6627	Pnma
Larnite (β-C_2S)	C_2S	Ca_2SiO_4	81096/–	P121/n1
α′-C_2S	C_2S	Ca_2SiO_4	81097/–	Pnma
α-C_2S	C_2S	Ca_2SiO_4	81099/–	P63/mmc
Hatrurite	C_3S	Ca_3SiO_5	–/01-070-8632	Cm
Lime	C	CaO	28905/–	Fm-3m
Portlandite	CH	$Ca(OH)_2$	–/01-076-0571	P-3m1
Calcite	Cc	$CaCO_3$	80869/–	R-3cH
Others				
Ferrite (Iron-met.)	–	Fe	76747/–	Im-3m
Fe-Perovskite	C(F,T)	$CaTi_{0.65}Fe_{0.35}O_{2.825}$	–/04-019-5637	Pnma

samples" and six coarser samples (4–5.6 mm) referenced as "C" or "C-Type samples" are analyzed that were derived by sieving the bulk samples. The reason for the addition of these samples is that a larger range of FeO/Fe_2O_3 and degree of weathering is covered because finer fractions of BOF slag are more oxidized (i.e. lower FeO/Fe_2O_3) and weathered compared to coarser fractions BOF slag fractions [31]. Therefore these samples were added to the study in order to cover this extended range of phase composition.

2.2. XRF analysis

The XRF analysis on BOF slag samples follows a procedure involving two different steps. In a first step the sample is heated up to 1000 °C in order to remove volatiles and the loss on ignition (LOI) is recorded. In a second step, fused beads were produced by using lithium borate ($Li_2B_4O_7$:$LiBO_2$ = 65:35) in weight proportions of sample to borate 1:10. The analysis of samples is performed on a PANalytical Axios quantifying the components Al_2O_3, CaO, Cr_2O_3, MgO, MnO, P_2O_5, SiO_2, TiO_2, V_2O_5 and Fe total.

2.3. Fe redox titration

Earlier studies already reported that Fe can be present in three different Fe species (Fe(0), Fe(II) and Fe (III)) in BOF slag [19,32,33]. In order to quantitatively determine the different Fe species for each sample, redox titration method is used based on bromine-methanol titrimetric method and titration with potassium dichromate, respectively. Fe(0) and Fe (II) are subsequently determined according to ISO 5416-2006 and ISO 9035:1989. The titration results are used to calculate Fe(III) by difference from Fe total determined by XRF.

2.4. XRD analysis

Prior to the analysis further sample preparation is necessary for the quantitative phase analysis with the Rietveld method [27]. To all samples exactly 10 wt% Si-metal (3.6 g sample and 0.4 g Si-Standard) is added as internal standard. In order to receive reproducible results, it is necessary to mill the material to a grain size below 10 μm [27]. This is achieved using a Retsch McCrone micronizer and a milling time of 20 min adding of cyclohexane (7 ml). Samples were dried for 5 min at 70 °C in a furnace, and back-loaded on metal sample holders for XRD analysis. The median grainsize obtained for all samples was D50 = ~5 μm.

For the XRD measurement Co-radiation is preferred over Cu-radiation in order to avoid microabsorption with the Fe-rich samples [27,28,34]. XRD measurements were performed on a Malvern PANalytical XpertPro equipped with a Co-tube ($K\alpha_1$ 1.7901 Å, $K\alpha_2$ 1.7929 Å) and Pixel 3D detector. The measurements were performed with a fixed divergence slit setting of 0.5° and 0.04 rad soller. The 2Theta range of the measurement was 10–120°.

2.5. Rietveld quantitative phase analysis

For Rietveld quantitative phase analysis (RQPA) a total of 14 phases (including Si-standard) was taken into account (Table 4). These 14 phases and structures were used based on previous experience with RQPA of BOF slag at Tata Steel IJmuiden. Two RO-Phases were used in the quantification in order to account for solid solution in this phase (FeO – MgO – MnO – CaO) [25,26,35]. Three polymorphs of C_2S (β-C_2S, α′-C_2S and α-C_2S) were included in the quantification although only two C_2S polymorphs (β-C_2S, α′-C_2S) are usually reported in the literature [9,35–37]. In the Rietveld quantification, α-C_2S never exceeds a total of 2.5 wt%. Table 4 reports the used structures from the database ICDS or PDF and their respective stoichiometry for the Rietveld quantitative phase analysis.

3. Modelling approach

3.1. Classical Bogue equations for OPC

The classical Bogue equations were developed and published by Bogue in 1929 [1] and are also part of the standard speciation for OPC in the ASTM Standards (ASTM C150) [38]. The Bogue equations are used as an orientation for the modelling approach of the BOF slag phase quantities. Hence, the Bogue equations that are currently used in the ASTM C150-09 are repeated here. The Bogue equations assume that the major clinker oxides CaO, SiO_2, Al_2O_3 form the clinker phases C_3S, C_2S, C_3A and C_4AF. Moreover, SO_3 is combined to $C\overline{S}$ and MgO is uncombined and forms periclase (MgO). By performing a molar balancing of the oxides CaO, SiO_2, SO_3, Al_2O_3 and Fe_2O_3 the molar quantities of the major clinker phases (C_3S, C_2S, C_3A, C_4AF and $C\overline{S}$) can be derived from the Equation Sequence 1 [39].

$$n_{C_4AF} = n_F$$

$$n_{C_3A} = n_A - n_F$$

$$n_{C\overline{S}} = n_{\overline{S}}$$

$$n_{C_3S} + n_{C_2S} = n_S$$

$$3n_{C_3S} + 2n_{C_2S} + 3n_{C_3A} + 4n_{C_4AF} + n_{C\overline{S}} = n_C$$

$$\rightarrow n_{C_3S} = n_C - (2n_S + 3n_A + n_F + n_{\overline{S}})$$

$$n_{C_2S} = n_S - n_{C_3S}$$

Equation Sequence 1 gives the molar balancing equations to describe the formation of the major clinker phases C_3S, C_2S, C_3A and C_4AF [35].

Using the molar masses for the oxides (Table 5) in question the equations can be rewritten, so that the oxide masses can be used in the equations (Equation Sequence 2). This has the purpose to derive the phase quantities in wt% directly from the oxide wt%.

$$x_{C_4AF} = 3.043\ x_F$$

$$x_{C_3A} = 2.650\ x_A - 1.692\ x_F$$

$$x_{C_3S} = 4.072\ x_C - (7.6\ x_S + 6.718\ x_A + 1.43\ x_F + 2.852\ x_{\overline{S}})$$

$$x_{C_2S} = 2.867\ x_S - 0.754\ x_{C_3S}$$

$$x_{C\overline{S}} = 1.701\ x_{\overline{S}}$$

Equation Sequence 2 presents the classical cement Bogue equations as standardized in ASTM C150 which gives the wt% of the major clinker phases by using the wt% of oxides. For reasons of completion the equation for $C\overline{S}$ is added, which is omitted in the ASTM C150. Also, it should be noted that within the ASTM C150 free CaO is not deducted, whereas it was initially performed by Bogue.

Taylor [40] already pointed out that the Bogue equations are a simplification and may give incorrect values and that the Bogue equations may not represent the actual phase compositions due to the fact that during the clinker cooling procedure equilibrium is not maintained. This results in overestimating C_2S and under estimating C_3S amounts. Moreover, the Bogue equations only assume pure phases or in case of C_4AF a constant stoichiometry, which is not true in reality [40]. That is the main reason errors occur. However, the Bogue equations are still widely used today which is evidenced by the fact that the Bogue equations are contained within ASTM C150. The authors would like to note here that in the ASTM C150 $C\overline{S}$ is omitted, whereas it was initially included in the original Bogue equations [1,38].

3.2. Framework conditions for the BOF slag model

Every modelling approach has a different aim. In this study, the aim is to predict the BOF slag phase quantities with respect to the main phases. Moreover, before modelling the BOF slag composition one needs to understand that BOF slag is a highly variable industrial by-product due to the fact that it is produced in batched and that steel companies [41] are primarily concerned with the composition of the steel which translates to the BOF slag composition. As there are many different steel compositions there are many resulting BOF slag compositions, which may not only differ between steel plants [10,42] but also within the production of a single steel plant [14]. For example, CaO and SiO_2 of investigated BOF slags vary between 34 to 57 wt% and 7.7 to 36 wt%, respectively [10]. Consequently, BOF slag phase composition will vary widely. However, the modelling aims to predict phase compositions for common BOF slags rather than more extreme chemical compositions. As common BOF slag composition, we propose the following definition: The average chemical composition values BOFS as reported in [10] ±5 wt% (Table 1). Moreover, it should be clarified that BOF slag production of a steel plant may be very stable (±3 wt% CaO) if single converter heats are accumulated over a longer period of time (>one week) and processed together.

Table 5
Oxides with their respective cement notation and their respective molar masses.

Oxide	Oxide cement notation	Molar mass (g/mol)
CaO	C	56.08
SiO_2	S	60.08
Al_2O_3	A	101.96
Fe_2O_3	F	159.69
FeO	f	71.84
MgO	M	40.3
MnO	m	70.94
P_2O_5	P	141.94
TiO_2	T	79.87
V2O5	V	181.88
Cr_2O_3	Cr	151.99
SO_3	$\overline{S}$	80.06

Moreover, even though OPC and BOF slag show certain similarities in the chemical and phase composition [10] and both are crystalline materials with initially very low amorphous content (<5 wt%) [3,43], the modelling approach is somewhat different. In OPC, only one Fe species is present (Fe3+, i.e. Fe2O3), which is only incorporated in C2(A,F). This is in complete contrast to BOF slag, because in BOF slag Fe is present in three different species, which is in the form of metallic Fe, FeO and Fe_2O_3 (Fe^0, Fe^{2+} and Fe^{3+}, respectively). The different Fe species in BOF slag are incorporated in C_2(A,F), RO-Phase, Ff and metallic Fe. The metallic Fe is usually around 1 wt% because it is impossible to recover all metal droplets from the BOF slag [44]. The FeO/Fe_2O_3 ratio in BOF slag may vary widely (at least 0.6–6.8 by mass) [45,46], even steel plant internally as it will be shown, where multiple heats supposed to dampen out the chemical variability and constantly comparable cooling methods are applied. Furthermore, the Fe speciation cannot be simply determined by XRF and is usually determined by dichromate titrimetry [47].

As a common BOF slag chemical composition is defined, it is necessary to understand the common BOF slag phase assemblage and the origin of certain phases. Since we use a Bogue approach, cement notation will be used for the phase names rather than the more commonly used mineral names (Table 2) in the literature. The most common phases in BOF slag are C_2S, C_2(A,F), RO, f-C, Ff. Other phases that may occur are C_3S, CF (Fe-Perovskite), Cc and CH. In order to predict the phase assemblage it is necessary to understand how these phases form. Cc and CH are unstable above 1000 °C whereas a basic oxygen furnace operates at significantly higher temperatures (>1500 °C), so CH and Cc are unstable under these conditions. CH and Cc would lose their volatile content (i.e. CO_2 and H_2O, respectively), form f-C and do not exist as primary phases in BOF slag. Therefore, it can be stated that Cc and CH are weathering products from C_2S and f-C which has been previously confirmed by [41]. Due to the fact that these phases are secondary weathering products, which heavily depend on storage conditions (i.e. climate and grain size distribution), Cc and CH are excluded from the modelling of the phase assemblage. The presence of C_3S mainly depends on the cooling conditions and CaO content [14,32] in the BOF slag. However, C_3S tends to decompose to C_2S and f-C in the slag due to its slow cooling during industrial processing. Additionally the CaO values considered in this model are generally lower than 47 wt% which is given by [14] as the boundary for the presence of significant amounts of C_3S (>3 wt%). Therefore, C_3S is ignored in the modelling calculations. Another phase that is a secondary phase is Ff also known as magnetite, which forms under oxidizing conditions. The formation of Ff mainly depends on the cooling conditions during processing of the BOF slag [15,36,48] since Ff is unstable under basic oxygen furnace conditions [49]. f-C has three origins in BOF slag under industrial cooling conditions: i) undissolved flux particles [50,51], ii) exsolution from C_3S that forms together with C_2S and iii) interstitial f-C that forms at the end of the crystallization sequence [51]. Since these origins do not solely depend on the total CaO content but also on the cooling conditions and oxygen blowing time in the basic oxygen furnace it may be that the f-C content is very variable and problematic to predict. However, this is probably more valid for BOF slags with high CaO (>47 wt%) and more uncommon cooling methods (e.g. air granulation), for which the presented model will have its limitations. C_2S is the most

dominant phase in BOF slag (>35 wt%) and occurs generally in two polymorphs β-C_2S and α′-C_2S [13]. In the presented modelling approach, both polymorphs are generalized as C_2S. The RO-phase which is often referred to as wuestite in the literature is a solid solution of FeO, MgO, MnO and minor amounts of CaO (<5 wt%) [10,14,52]. To summarize, based on the typical chemical compositions that are assumed and the slow cooling conditions that are applied generally in the industry, the modelled phase assemblage consists of C_2S, RO-phase, C_2(A,F), Ff and f-C.

In the next step it will be assessed, which oxides are included in which phases or form solid solutions. This step is necessary in order to assign the oxides to their respective phases. For simplicity reasons, minor oxides (<5 wt% of the bulk BOF slag composition) such as V_2O_5 or TiO_2 are assigned to a single phase. The RO-phase is a solid solution of MgO, FeO, MnO and minor amounts of CaO (<5 wt%). Also, most of the Cr_2O_3 is incorporated in the RO-Phase and hence the modelling assumes that all Cr_2O_3 MgO and MnO are incorporated in to the RO-Phase [32]. In order to not over complicate the first modelling approach, it is assumed that the RO-phase does not contain any CaO. For the same reasons, it is assumed that Ff consists of pure Fe_2O_3 and FeO [13,53,54]. Moreover, C_2(A,F) contains parts of the CaO and Fe_2O_3 and all of the Al_2O_3 and TiO_2 even though small amounts of Al_2O_3 and TiO_2 are partially incorporated into C_2S as well [13,53,54]. C_2S includes all SiO_2, P_2O_5 and V_2O_5 and major parts of the CaO as C_2S, C_3P and C_3V form a solid solution system. An overview for the assignment of the oxides to the modelled phases is given in (Table 6).

In order to calculate a f-C at the end of the modelling sequence it is necessary to assume that a certain portion of the Fe^{total} (i.e. the sum of Fe^0, Fe^{2+} and Fe^{3+}) is incorporated into C_2(A,F) as Fe^{3+}. This Fe^{3+} was formed during the basic oxygen furnace process. The remaining Fe^{3+} is used to form the secondary Ff phase and was formed during the cooling process. However, the portion of the initial Fe^{3+} that is incorporated into C_2(A,F) is dependent on the Fe^{total} and the exact portion is unknown. However, from internal reports of the Tata Steel plant IJmuiden, it is known that the initial Fe^{3+}/Fe^{total} in the basic oxygen furnace varies between 0.25 and 0.33. Hence, the BOF slag phase composition is modelled with three Fe^{3+}/Fe^{total} ratios (0.25, 0.292 and 0.33) and form the equation of a positive regression line. The positive regression line (Appendix Fig. 1) is determined by two points, which are the lowest and highest Fe^{total} values of the data set (17.6 and 21.1 wt%) and match the assumed lowest and highest assumed initial Fe^{3+}/Fe^{total} (0.25 and 0.33) which is all incorporated in C_2(A,F). The resulting equation is expressed as follows:

$$\omega_i = X\,Fe_i^{total} * 0.02313 - 0.15788 \quad (1)$$

With ω_i is the initial Fe^{3+}/Fe^{total} and X Fe_i^{total} is the amount of Fe^{total} in mass. Eq. (1) is used to model the amount of Fe_2O_3 that is used to form the Fe containing endmember of C_2(A,F), whereas the remaining Fe_2O_3 is assumed to be formed secondarily and hence determines the amount of Ff. The used ω_i ratios are reasonable choices based on the work of Schürmann et al. [55] on the relationship between FeO and Fe_2O_3 contents in BOF slag. Due to the unknown ω_i ratio in the BOF slag, it is decided to use the aforementioned ratios and quantitatively asses the modelled values.

Table 6
Assignment of oxides to the BOF slag phases.

Phases	Oxides
C_2S	$CaO\text{-}SiO_2\text{-}P_2O_5\text{-}V_2O_5$
C_2(A,F)	$CaO\text{-}Al_2O_3\text{-}Fe_2O_3\text{-}TiO_2$
Ff	$Fe_2O_3\text{-}FeO$
RO-Phase	$FeO\text{-}MgO\text{-}MnO\text{-}Cr_2O_3$

3.3. The Bogue approach applied to BOF slag

From the presented frame work conditions above Equation Sequence 3 can be drawn:

$$n_{C_2S\ (total)} = n_{C_2S} + n_{C_3P} + n_{C_3V}$$

$$n_{C_2(A,F)} = n_{C_2F} + n_{C_2A} + n_{C_2T}$$

$$n_C = n_{freeC} + 2n_{C_2S} + 3n_{C_3P} + 2n_{C_2F} + 2n_{C_2A} + 2n_{C_2T} + 3n_{C_3V}$$

$$\rightarrow n_{C_2F} = \omega_i{}^* n_{Fe^{total}}$$

$$\rightarrow n_{Ff} = n_F - n_{C_2F}$$

$$\rightarrow n_{RO} = \left(n_f - n_{Ff}\right) + n_M + n_m + n_{Cr}$$

$$\rightarrow n_{f-C} = n_C - \left(2n_{C_2S} + 3n_{C_3P} + 3n_{C_3V} + 2n_{C_2A} + 2n_{C_2F} + 2n_{C_2T}\right)$$

Equation Sequence 3 gives the molar balancing equations to describe the formation of the major BOF slag phases C_2S, C_2(A,F), Ff and RO-Phase. ω_i is the initial Fe^{3+}/Fe_{total}. It should be noted that f-C is the remaining CaO at the end of the equations as the unbound CaO.

The Equation Sequence 3 may be transferred to mass proportions by using the oxide constituent atomic mass proportion in a certain phase as Bogue did [1]:

$$X_{C_2S\ (total)} = 2.867\,X_S + 2.185\,X_P + 1.925\,X_V$$

$$X_{C_2(A,F)} = 2.434{}^*\omega_i{}^* X_{Fe\ total} + 2.1\,X_A + 2.404\,X_T$$

$$X_{Ff} = 1.45{}^*(X_F - (0.587{}^*(2.434{}^*\omega_i{}^* X_{Fe\ total})))$$

$$X_{RO} = \left(X_f - 0.31\,X_{Ff}\right) + X_M + X_m + X_{Cr}$$

$$X_{f-C} = X_C - (1.867\,X_S + 1.185\,X_P + 0.925\,X_V + 1.1\,X_A + 1.404\,X_T + 1.004{}^*\omega_i{}^* X_{Fe\ total})$$

Table 7
Seven quantitative model assessment measures with their expressions in the text, their formulation and the desired value for an ideal model.

Expression	Formulation	Desired Value
a	See footnote	0
b	See footnote	1
SSPE	$SSPE = \sum_{i=1}^{n}(y_i - \hat{y}_i)^2$	0
U_b	$U_{bias} = \left[n(Y - \hat{Y})^2\right] / SSPE$	0
U_s	$U_{b=1} = \left[(b-1)^2 \sum_{i=1}^{n}(\hat{y}_i - \hat{Y})^2\right] / SSPE$	0
U_e	$U_{error} = \sum_{i=1}^{n}(est_i - y_i)^2 / SSPE$	1
RMSD	$RMSD = \sqrt{\frac{1}{n-1}^{*} SSPE}$	0

Footnote: a and b are the expressions for the intersection with the y-axis and the slope factor, respectively, of the fitted regression line through the points determined by RQPA and Bogue BOF slag. U_e is usually referred as R^2 of the fitted regression. y_i is the value for the observed value of one point (i.e. RQPA) and $\hat{y}_i$ is the modelled value of a point (i.e. Bogue BOF slag). Y is the mean of the observed values (i.e. RQPA) and $\hat{Y}$ is the mean of the modelled values (i.e. Bogue BOF slag).

Equation Sequence 4 gives the wt% of the major BOF slag phases by using the wt% of oxides (Bogue equation).

With these equations one can derive directly the phase wt% from the oxide wt%, without the conversion to mol% (Equations Sequence 4). Therefore these equations are easily applicable to any average oxide composition data of BOF slag.

3.4. Quantitative model assessment

In order to evaluate the accuracy of the model the advice of Piñeiro et al. [56] is followed. In total 7 different measures (Table 7), were used to quantitatively asses the deviations of the modelled values from the RQPA data. This will help to understand the properties of the model and potential deviations from the RQPA data. A brief explanation of the 7 different measures for the model assessment is described in the appendix and an in-depth explanation can be found in [56,57]. The 7 different measures for the model assessment are not only calculated for the total model fit of all samples and different ω_i that is incorporated in $C_2(A,F)$ (i.e. 0.25, 0.292, 0.33 and variable ω_i) but also for each individual phase (C_2S, $C_2(A,F)$, RO-Phase and f-C). The modelled f-C quantities are excluded from the total model assessment because they are most likely altered due to effect of weathering forming CH (portlandite), Cc (calcite) and possible amorphous content. To avoid confusion for the reader the specific model assessment parameter of a phase or the total is indicated by superscript (e.g. U_b^{C2S}). The application of different measures of for the model assessment will help to interpret the model and identify where the model would need improvements.

4. Results and discussion

4.1. Effect of grain size on the chemical and phase composition

Tables 8 and 9 present the chemical composition and RQPA results of the BOF slag samples that are used for assessing the accuracy of the Bogue BOF slag model. The sample type (B, C and F) has significant influence on the reported phase proportions. RQPA C_2S values for the F-type samples are the significantly lower compared to B and C-type samples. For example F16 – F20 have a mean C_2S of 32.6 wt%, whereas B16 – B21 have an average of 40.7 wt% and C16 – C21 an average of 42.8 wt%. The reason behind the positive correlation between particle size and C_2S is that C_2S tends to be effected by weathering processes of BOF slag which is more pronounced for higher surface areas and smaller grain sizes [58]. These weathering products also tend to accumulate in the smaller fractions due to their size [41]. This is also confirmed by the higher amount of weathering products (WP; i.e. sum of Cc, CH and amorphous) in the F-type samples, which is 15.1 wt% on average (F16 – F20) compared to a mean of 1.9 wt% WP (B16 – B20) of B-type samples. The RQPA results for the RO-Phase and Ff amounts showing decreased and increased phase amounts, respectively, from C-type over B-type to F-type samples, which reflects the gradual effect of oxidation through the sample suite. As it is also shown by the Fe_2O_3/Fe^{total} for C-Type, B-Type and F-Type samples (16–21), which is on average 0.55, 0.61 and 0.84, respectively. The increase in Fe_2O_3/Fe^{total} from coarser to finer grain sizes was already observed by [31,59]. RQPA results of $C_2(A,F)$ seem to be unaffected by oxidation and weathering with F16 – F20 samples have a mean of 18.8 wt%, B16 - B20 have a slightly higher mean of 19.6 wt%.

4.2. Effect of varying initial Fe^{3+}/Fe^{total} (ω_i) on the phase quantities

The presented Bogue BOF slag equations are applied here to the combined chemical composition data measured with XRF and Fe titration (Table 8) to derive phase quantities (Appendix Tables 1–4), which are the compared to the RQPA data in Fig. 1. The first step is to evaluate the modelled data with different ω_i to see its effect. The modelled phase quantities for four selected ω_i are presented together with the RQPA results in Fig. 1.

The modelled phase quantities for four selected ω_i (0.25, 0.292, 0.33

Table 8
Combined chemical composition determined by XRF and Fe redox titration of all BOF slag samples used in this study.

Sample ID	Al_2O_3	CaO	Cr_2O_3	Fe_2O_3	FeO	Met. Fe	MgO	MnO	P_2O_5	SiO_2	TiO_2	V_2O_5	Total	Fe total	LOI	$LOI_{Fe\text{-}corr.}$
B1	1.8	41.6	0.3	13.7	10.1	1.0	7.8	4.8	1.7	14.4	1.5	1.1	100	18.4	−1.2	0.8
B2	1.7	42.6	0.3	11.4	11.6	1.1	8.0	4.5	1.6	14.6	1.5	1.2	100	18.0	−1.2	1.1
B3	2.0	41.2	0.3	13.1	11.7	1.3	7.7	4.6	1.6	14.1	1.4	1.0	100	19.4	−1.3	1.1
B4	1.9	41.5	0.3	12.7	12.1	1.1	7.9	4.3	1.6	14.5	1.3	0.9	100	19.2	−0.8	1.5
B5	1.9	40.8	0.3	13.4	10.7	1.9	8.1	4.6	1.7	13.7	1.6	1.3	100	19.4	−1.1	1.7
B6	1.9	41.6	0.3	9.2	13.8	1.9	7.9	4.7	1.8	13.9	1.6	1.4	100	18.9	−1.8	1.4
B7	1.8	41.0	0.3	11.0	13.9	1.1	7.8	4.7	1.8	13.6	1.7	1.4	100	19.3	−1.6	1.0
B8	2.7	39.8	0.3	10.7	15.1	1.2	7.9	4.3	1.7	13.5	1.5	1.3	100	20.3	−2.0	0.8
B9	2.0	40.9	0.3	11.6	14.0	0.7	8.0	4.3	1.8	13.5	1.5	1.4	100	19.7	−1.8	0.5
B10	2.2	40.8	0.3	10.4	14.2	1.2	8.1	4.3	1.7	13.8	1.6	1.4	100	19.5	−1.9	0.8
B11	2.4	40.9	0.3	10.4	13.6	1.2	8.9	4.3	1.6	13.5	1.6	1.3	100	18.9	−1.5	1.1
B12	2.4	39.4	0.3	11.9	13.9	1.4	8.8	4.3	1.6	13.2	1.5	1.2	100	20.4	−1.6	1.2
B13	2.1	42.0	0.3	10.9	11.3	1.4	9.0	4.6	1.6	13.9	1.6	1.2	100	17.7	−1.3	1.2
B14	1.7	42.5	0.3	8.9	12.8	1.8	8.3	4.9	1.6	14.2	1.7	1.3	100	17.9	−1.7	1.3
B15	1.8	42.0	0.3	9.3	13.5	1.1	8.4	4.6	1.6	14.3	1.6	1.4	100	18.0	−1.7	0.8
B16	1.8	41.7	0.3	10.4	11.7	2.2	8.5	4.6	1.5	14.2	1.6	1.3	100	18.4	−1.3	1.8
B17	1.9	41.6	0.3	11.2	11.8	1.6	8.4	4.7	1.5	13.9	1.6	1.4	100	18.5	−1.2	1.5
B18	2.0	40.3	0.3	15.0	8.9	2.6	8.6	4.3	1.5	13.5	1.5	1.4	100	20.0	−1.4	1.7
B19	2.0	41.1	0.3	11.4	12.6	1.1	8.4	4.7	1.6	13.8	1.6	1.3	100	18.7	−1.2	1.2
B20	1.9	41.9	0.3	10.3	12.6	2.0	8.4	4.5	1.4	14.1	1.4	1.2	100	18.7	−1.5	1.6
B21	2.2	41.1	0.3	10.3	13.0	1.5	8.9	4.4	1.4	14.1	1.5	1.3	100	18.7	−1.4	1.4
C15	1.9	40.9	0.3	10.8	12.7	1.7	8.3	4.7	1.6	14.1	1.6	1.5	100	19.1	−2.1	0.8
C16	1.9	42.3	0.3	9.8	12.2	1.3	8.6	4.7	1.5	14.5	1.7	1.4	100	17.6	−1.9	0.6
C17	1.9	41.7	0.3	10.7	12.4	1.2	8.6	4.7	1.5	14.0	1.6	1.4	100	18.3	−1.9	0.6
C18	2.0	41.2	0.3	10.0	13.9	1.2	8.8	4.4	1.6	13.9	1.6	1.4	100	18.9	−2	0.6
C19	2.0	40.6	0.3	8.8	15.1	1.8	8.4	4.7	1.6	13.7	1.6	1.3	100	19.6	−2.2	1.1
C21	2.3	41.1	0.3	11.0	12.2	1.2	8.8	4.4	1.5	14.4	1.5	1.4	100	18.4	−2.2	0.2
F16	2.1	41.3	0.3	15.5	7.4	3.0	8.4	4.5	1.4	13.3	1.6	1.3	100	19.6	0.6	3.8
F17	2.5	42.6	0.3	15.6	7.0	1.6	8.5	4.4	1.4	13.3	1.5	1.3	100	17.9	2.9	5.0
F18	2.2	40.0	0.3	14.9	8.4	4.1	8.1	4.2	1.4	13.5	1.5	1.3	100	21.1	1.5	5.7
F19	2.5	40.9	0.3	18.7	6.0	2.0	8.1	4.4	1.4	12.8	1.5	1.3	100	19.8	2.4	4.6
F20	2.3	42.3	0.3	15.8	6.7	2.2	9.0	4.2	1.3	13.5	1.4	1.1	100	18.5	2.5	5.0

Table 9
RQPA results for the BOF slag samples together with the Goddess of Fit (GOF) and weighted profile R-factor (Rwp).

Sample ID	RO-Phase	Ff	$C_2(A,F)$	C_2S	C_3S	f-C	CH	Cc	Others	Amorphous	Total	GOF	Rwp
B1	24.1	8.2	20.6	40.3	0.8	1.1	0.1	0.4	0.4	4.0	100	1.24	1.89
B2	25.0	6.8	20.7	43.8	0.7	1.9	0.1	0.3	0.8	0.0	100	1.24	1.93
B3	25.4	7.7	21.8	39.8	0.5	1.5	0.2	0.3	0.2	2.6	100	1.22	1.87
B4	24.9	6.6	19.6	40.4	0.8	1.4	0.4	0.6	0.2	5.2	100	1.25	1.93
B5	23.0	8.3	19.5	38.4	0.9	1.2	0.5	0.5	0.6	7.0	100	1.22	1.86
B6	28.6	5.0	21.0	40.9	1.0	1.6	0.1	0.2	0.6	0.9	100	1.23	1.88
B7	26.1	5.4	20.1	39.1	0.9	1.1	0.1	0.4	0.8	6.1	100	1.26	1.82
B8	30.0	5.2	21.4	38.6	0.7	1.2	0.1	0.2	0.8	1.8	100	1.24	1.87
B9	26.8	5.9	20.3	38.6	0.6	1.5	0.2	0.4	0.5	5.2	100	1.26	1.83
B10	28.2	4.7	21.1	37.9	0.8	1.4	0.1	0.2	0.5	5.2	100	1.27	1.84
B11	28.3	4.8	20.3	38.8	0.7	1.5	0.1	0.3	0.4	4.8	100	1.23	1.89
B12	28.9	6.3	18.9	39.0	0.8	1.0	0.9	0.3	0.7	3.2	100	1.19	1.87
B13	25.0	5.6	20.1	41.8	0.4	1.9	0.1	0.4	0.5	4.3	100	1.22	2
B14	28.9	4.4	19.2	42.5	0.6	2.0	0.2	0.1	0.4	1.7	100	1.22	1.81
B15	28.3	4.6	19.2	42.5	0.6	1.6	0.1	0.3	0.2	2.6	100	1.24	1.76
B16	26.2	5.5	18.8	40.9	0.7	1.3	0.1	0.2	0.5	5.9	100	1.18	1.95
B17	26.5	6.4	20.1	42.6	0.5	1.8	0.4	0.4	0.5	0.8	100	1.21	1.98
B18	27.6	5.8	20.6	39.7	0.8	1.4	0.1	0.7	0.9	2.3	100	1.18	1.92
B19	28.1	7.0	20.2	41.4	0.5	1.6	0.0	0.2	1.0	0.0	100	1.28	1.49
B20	27.9	6.3	18.3	44.2	0.5	1.8	0.0	0.1	0.8	0.0	100	1.29	1.51
B21	28.0	6.8	19.4	43.2	0.5	1.5	0.0	0.2	0.5	0.0	100	1.29	1.51
C15	28.1	5.2	20.8	41.7	0.6	1.2	0.0	0.1	0.5	1.8	100	1.19	1.94
C16	28.5	5.0	18.9	43.9	0.6	1.7	0.6	0.1	0.6	0.0	100	1.17	1.94
C17	27.8	5.1	17.9	44.4	0.8	1.6	0.8	0.5	1.1	0.0	100	1.2	1.97
C18	28.7	4.4	19.2	41.1	0.6	1.5	0.8	0.1	0.6	3.0	100	1.2	1.97
C19	31.4	4.5	18.9	42.4	0.2	1.3	0.1	0.1	1.0	0.0	100	1.3	1.51
C21	30.6	4.9	17.5	43.2	0.6	1.6	0.1	0.1	1.3	0.0	100	1.31	1.54
F16	17.9	10.9	19.8	33.9	1.4	1.6	0.1	1.4	1.8	11.3	100	1.24	2.02
F17	16.8	11.6	18.1	32.6	0.6	1.0	1.2	1.9	1.5	14.7	100	1.23	2.05
F18	20.1	11.7	18.4	30.9	1.3	1.1	0.8	2.2	2.0	11.5	100	1.27	2.03
F19	16.8	13.1	19.7	31.7	0.2	1.1	0.8	1.5	1.4	13.7	100	1.34	1.57
F20	17.8	11.9	17.9	34.1	1.2	1.4	1.2	1.4	1.5	11.6	100	1.34	1.58

and variable) are presented in Fig. 1 (and in Appendix Tables 1–4) and show that the ω_i on the modelled C_2S contents has no influence, because C_2S is not allowed no incorporate Fe in the model and amounts solely rely on the SiO_2, P_2O_5 and V_2O_5 contents. In contrast, $C_2(A,F)$ is significantly influenced by the ω_i because $C_2(A,F)$ contents depend on the available Fe^{3+} set by the ω_i. Hence, the modelled $C_2(A,F)$ mean for the whole sample suite increases from 19.6 wt% ($\omega_i = 0.25$) to 23.3 wt% ($\omega_i = 0.33$). Consequently, the amount of Ff is influenced as well since the modelled amount relies on the remaining Fe_2O_3 content. At the lowest ω_i ratio the model gives an average of 7.3 wt% Ff for all samples. At the highest ω_i of 0.33, the model unrealistic (i.e. negative) values for one sample because not enough Fe_2O_3 is left over to form Ff. Therefore, the lower the ω_i is set the more Ff is formed. At the end this also has influence on the modelled amounts of the RO-Phase since it takes up the remaining FeO. Therefore, the means of modelled RO-Phase amounts increase on average from 22.7 wt% ($\omega_i = 0.25$) to 23.7 wt% ($\omega_i = 0.33$). The amount of calculated f-C is linked to the remaining CaO, after the CaO contained in C_2S and $C_2(A,F)$ is subtracted from the total CaO, consequently it is also influenced by the ω_i because with a higher ω_i more $C_2(A,F)$ is formed and hence less CaO is available to form f-C in the end. Therefore, f-C is the lowest at a ω_i of 0.33 with an average of 1.6 wt% and highest at a ω_i of 0.25 with an average of 3.2 wt%.

4.3. Quantitative model assessment of RQPA and Bogue BOF slag data

Table 10 reports the 7 different measures for the model assessment for the total sample set which includes the phases C_2S, $C_2(A,F)$, Ff and RO-Phase but ignores f-C. The decision to exclude f-C from the total model assessment is based on the fact that f-C is too altered by weathering and therefore outside factors for which no information is available. Also the measures for each single phase (C_2S, $C_2(A,F)$, Ff, RO-Phase, f-C) are reported. The values a^{total} and b^{total} for the fitted regression line of all phases are the best for a ω_i of 0.25 with 2.8 wt% and 0.847, respectively. Also U_b^{total} and $RMSD^{total}$ are the lowest at a ω_i of 0.25 with 0.305 and 3.8 respectively. The best U_e^{total} is found for a ω_i of 0.292 with 0.949 and the best U_S^{total} is given at the variable ω_i with 0.194. According to this evaluation it seems viable to conclude that a ω_i of 0.25 is the best to model the phase composition of the BOF slag since 5 of the 7 model assessment measures give the model agreement with the RQPA data. The model performs at a ω_i of 0.25 even better than variable ω_i even though the positive relation between higher Fe^{total} and higher Fe^{3+} is already reported [60].

As mentioned above, that modelled C_2S quantities do not change based on the ω_i, this has the effect that the model assessment measures do not change either. The parameters for the regression are not good since a^{C2S} and b^{C2S} differ significantly from the desired values of 0 and 1 with −65.4 wt% and 2.31, respectively. This deviation means that the linear correlation is biased and modelled values are generally too high and at lower C_2S values this deviation increases. This is also confirmed by the high U_b^{C2S} (0.82). However, U_e^{C2S} and U_s^{C2S}, with 0.653 and 0.067, respectively, show that a correlation between RQPA and modelled C_2S exist. Especially, the F-Type samples plot at the lower end of the regression line. As mentioned above, this is caused by the increased weathering of the F-Type samples. If the F-Type samples had similar SiO_2 and P_2O_5, they should disrupt this regression because SiO_2 and P_2O_5 are the determining factors for the amount of modelled C_2S. However, F16 – F20 have somewhat lower mean SiO_2 and P_2O_5 contents (13.28 and 1.37 wt%) than their coarser counterparts like the B-Type samples with a mean of SiO_2 and P_2O_5 of 13.95 and 1.48 wt%. This is also in agreement with Ashrit et al. [31] who reported that their finest fraction (<0.106 mm) of BOF slag was significantly lower in SiO_2 and P_2O_5 content. A possible tool to correct the modelled C_2S for weathering effects is by using LOI, which is determined prior to the XRF analysis.

The model assessment measures for $C_2(A,F)$ show that the regression between modelled $C_2(A,F)$ quantities and RQPA has a low $b^{C2(A,F)}$ (<0.175) and $U_e^{C2(A,F)}$ (<0.039), whereas the best model assessment measures are given with the variable ω_i. In contrast, the model assessment measures of $U_b^{C2(A,F)}$ and $RMSD^{C2(A,F)}$ are the best at an ω_i of 0.25

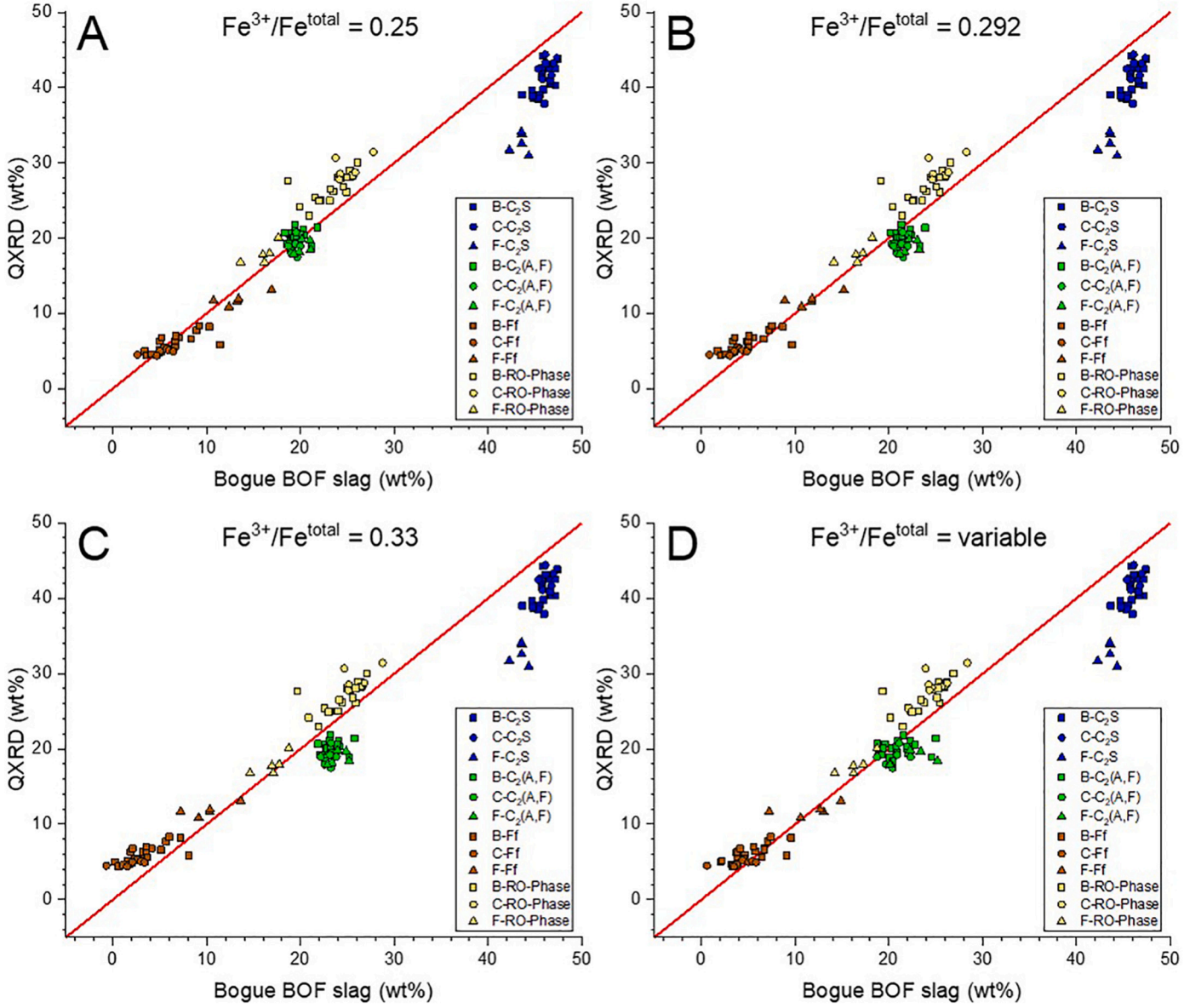

Fig. 1. A–D: Results of RQPA (y-axis) and computed Bogue BOF slag composition (x-axis) at different initial Fe^{3+}/Fe^{total} (0.25, 0.292, 0.33 and variable). The red solid line presents the 1:1 regression. (For interpretation of the references to colour in this figure legend, the reader is referred to the web version of this article.)

with <0.0001 and 1.28, meaning that the modelled phase quantities for $C_2(A,F)$ show little bias and have a low deviation from the RQPA values. To conclude, given that a variable ω_i achieves a better fit to the regression but the best values for $U_b^{C2(A,F)}$ and $RMSD^{C2(A,F)}$ are achieved with the lowest ω_i leads as for the total model assessment to the conclusion that a variable ω_i with lower and smaller range may be the best fit.

The model assessment measures of Ff show that again that a low ω_i is the best fit to model BOF slag phase composition. a^{Ff}, b^{Ff}, U_b^{Ff}, U_e^{Ff} and $RMSD^{Ff}$ are giving all the best values for an ω_i of 0.25. In contrast the model assessment measures b^{RO}, U_b^{RO}, U_e^{RO} and $RMSD^{RO}$ of the RO-Phase are all the best for a ω_i of 0.33, but are not significantly better than the same model assessment measures at a ω_i of 0.25. As for example RMSD values of $C_2(A,F)$, Ff and the total model assessment are the best at a ω_i of 0.25 but the RO-Phase deviates from that trend. It can be argued that the RO-Phase is generally underestimated with the Bogue BOF slag model (Fig. 1). This underestimation might not be due to the lack of FeO that is added to the RO-Phase at the end of the modelling sequence and decreasing U_b^{RO} and RMSD at higher ω_i, but because CaO incorporated into the RO-Phase is not taken into account during modelling. It is generally known that the RO-Phase in BOF slag may incorporate small amounts of CaO with variable amounts reported to be between 1 and 10 wt% [13,26,32].

The most significant findings of the quantitative model assessment are that:

i) At a ω_i of 0.25 the model gives the best fit to the observed RQPA values, although lower ω_i ratios have not been investigated.
ii) C_2S quantities are overestimated at all ω_i, which is probably due to weathering of the C_2S to form CH, Cc and amorphous.
iii) $C_2(A,F)$ and Ff are the least biased when modelled with a low ω_i of 0.25. However, the fit of the regression improves when a variable ω_i is used.
iv) The RO-phase is the least biased when the highest ω_i of 0.33 is applied, which contradicts to $C_2(A,F)$, Ff and the total model assessment. This might be related to the lack of CaO incorporation to the RO-Phase in the Bogue BOF slag model.

Table 10
Values for the calculated seven quantitative model assessment measures at different initial Fe^{3+}/Fe^{total} (i.e. ω_i). The total values exclude the phase f-C. The best value for a certain model assessment measure of a certain phase is highlighted by bold charaters.

Phase	Initial set Fe^{3+}/Fe^{total}	a	b	SSPE	U_b	U_s	U_e	RMSD
C_2S	0.25	−65.4	2.308	1298	0.82142	0.06730	0.653	6.47
	0.292	−65.4	2.308	1298	0.82142	0.06730	0.653	6.47
	0.33	−65.4	2.308	1298	0.82142	0.06730	0.653	6.47
	Vaiable	−65.4	2.308	1298	0.82142	0.06730	0.653	6.47
C_2(A,F)	0.25	16.4	0.166	**51**	**0.00000**	0.28305	0.015	**1.28**
	0.292	15.9	0.171	174	0.69762	0.09548	0.019	2.37
	0.33	**15.6**	**0.173**	496	0.88894	**0.03860**	0.023	4.00
	Vaiable	17.0	0.126	184	0.42899	0.37847	**0.039**	2.43
Ff	0.25	**1.8**	0.673	**80**	**0.12355**	0.46104	**0.825**	**1.61**
	0.292	2.9	0.675	109	0.35654	0.33400	0.823	1.88
	0.33	3.9	**0.676**	287	0.75558	**0.12535**	0.821	3.04
	Vaiable	2.8	0.653	107	0.18150	0.38070	0.755	1.86
RO−Phase	0.25	0.5	**1.116**	404	0.78412	**0.01273**	0.852	3.61
	0.292	−0.1	1.117	308	0.71778	0.01693	**0.853**	3.15
	0.33	−0.6	1.118	**237**	**0.63282**	0.02225	**0.853**	**2.76**
	Vaiable	**−0.1**	1.121	326	0.73086	0.01686	0.852	3.24
f−C	0.25	**1.1**	0.076	120	0.78042	**0.20218**	0.073	1.97
	0.292	1.3	0.078	53	0.49069	0.47074	0.081	1.31
	0.33	1.3	**0.080**	**29**	**0.03471**	0.89504	**0.086**	**0.97**
	Vaiable	1.6	−0.056	78	0.46548	0.68156	0.063	1.58
Total	0.25	**2.8**	**0.847**	**1832**	**0.04431**	0.32169	0.940	**3.80**
	0.292	3.1	0.829	1890	0.06739	0.41405	**0.949**	3.86
	0.33	3.6	0.803	2318	0.07680	0.47404	0.946	4.27
	Vaiable	4.7	0.790	5411	0.00018	**0.19411**	0.768	6.53

Based on these finding, the Bogue BOF slag model will be adjusted in the following paragraph and the new quantitative model assessment measures will be compared with the old ones.

4.4. Model improvement

In this paragraph the aim is the improvement of the initial Bogue BOF slag model in order to better adjust the modelled values to the observed RQPA values. In the first step, the focus is on the adjustment of C_2S. As pointed out before the high bias ($U_b^{C2S} = 0.821$ and $RMSD^{C2S} = 6.47$; Table 10) might be related to the weathered character of the BOF slag, because F-Type samples are significantly lower in C_2S compared to B and C-Type samples. C_2S forms CH, Cc and amorphous phase during weathering. Hence, it is suggested to correct the C_2S with the LOI, which is an indicator for the weathering degree. However, before finding any kind of relation it is necessary to correct the LOI for the mass gained by oxidation of metallic Fe and FeO to Fe_2O_3. If necessary a TG analysis under inert gas could determine the correct volatile content that is not influenced by the weight gain of the oxidation. The disadvantage of this method is additional analytical work. Hence, it is suggested to correct the LOI by calculating the weight increase from the oxidation of metallic Fe and FeO to Fe_2O_3. The Fe-corrected LOI is calculated according to:

$$LOI_{Fe-corr} = LOI_0 + \frac{X_f}{0.889} - X_f + \frac{X_{met.Fe}}{0.57} - X_{met.Fe} \quad (2)$$

whereas $LOI_{Fe\text{-}corr}$ is the Fe-corrected LOI, LOI_0 is the initially determine LOI and 0.889 and 0.57 are the constants that account for the mass increase from FeO and metallic Fe to Fe_2O_3, respectively. Fig. 2A presents the positive correlation between $LOI_{Fe\text{-}corr}$ and WP, which shows that the more the BOF slag is weathered the higher the $LOI_{Fe\text{-}corr}$. Moreover, Fig. 2B presents the negative correlation between $LOI_{Fe\text{-}corr}$ and C_2S determined by RQPA showing that it is possible to exploit the correlation between weathering character of the BOF slag and C_2S in order to correct the C_2S content by using the $LOI_{Fe\text{-}corr}$. For simplicity, the C_2S content is corrected by subtracting the modelled C_2S content by the

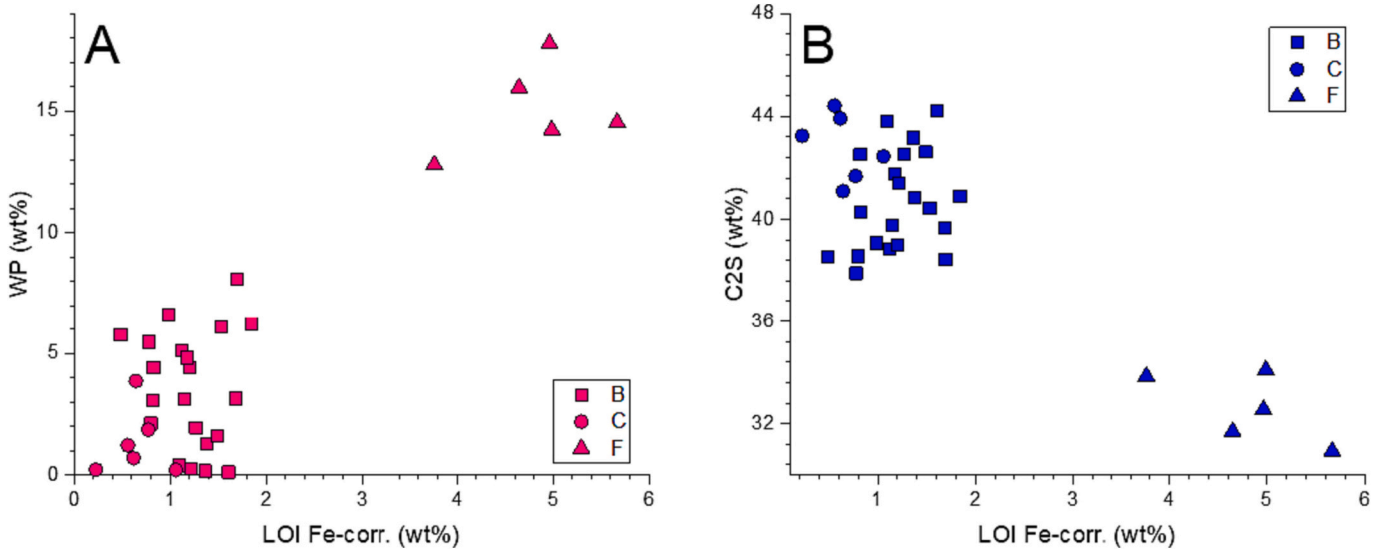

Fig. 2. A: $LOI_{Fe\text{-}corr}$ vs WP (sum of weathering products, i.e. CH, Cc and amorphous). B presents the $LOI_{Fe\text{-}corr}$ vs C_2S determined by RQPA.

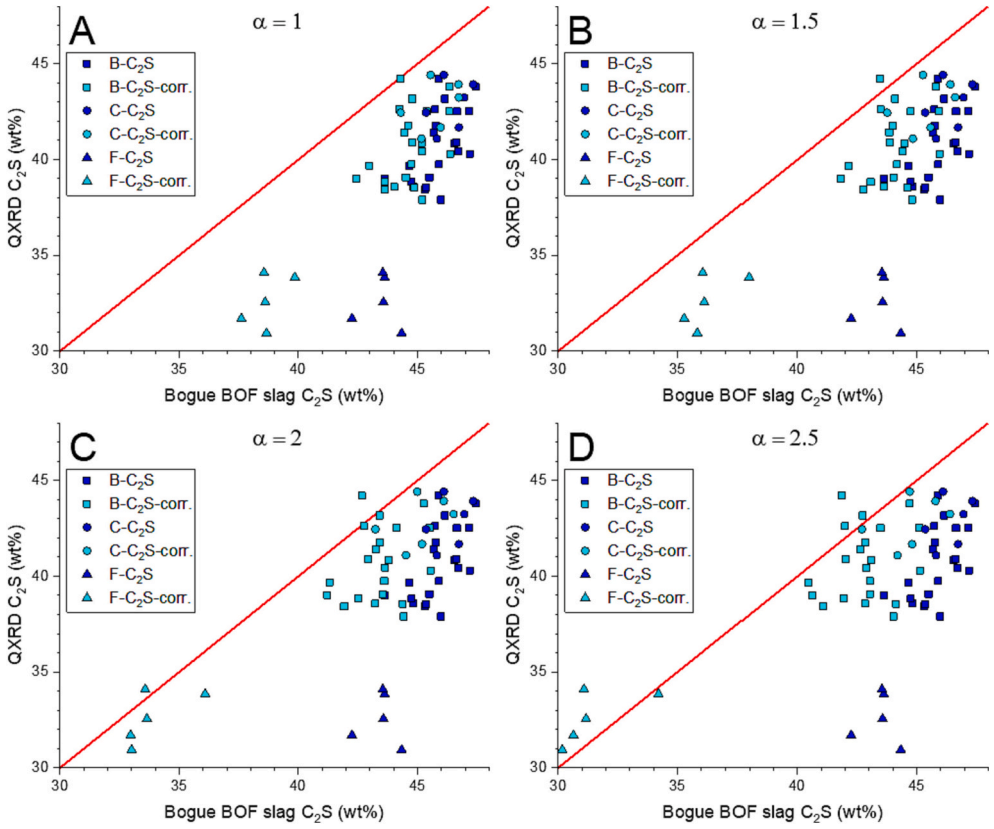

Fig. 3. A–D: Change of C_2S quantified by the Bogue BOF slag model by applying various correction factor α (1, 1.5, 2, and 2.5). The red solid line presents the 1:1 regression. (For interpretation of the references to colour in this figure legend, the reader is referred to the web version of this article.)

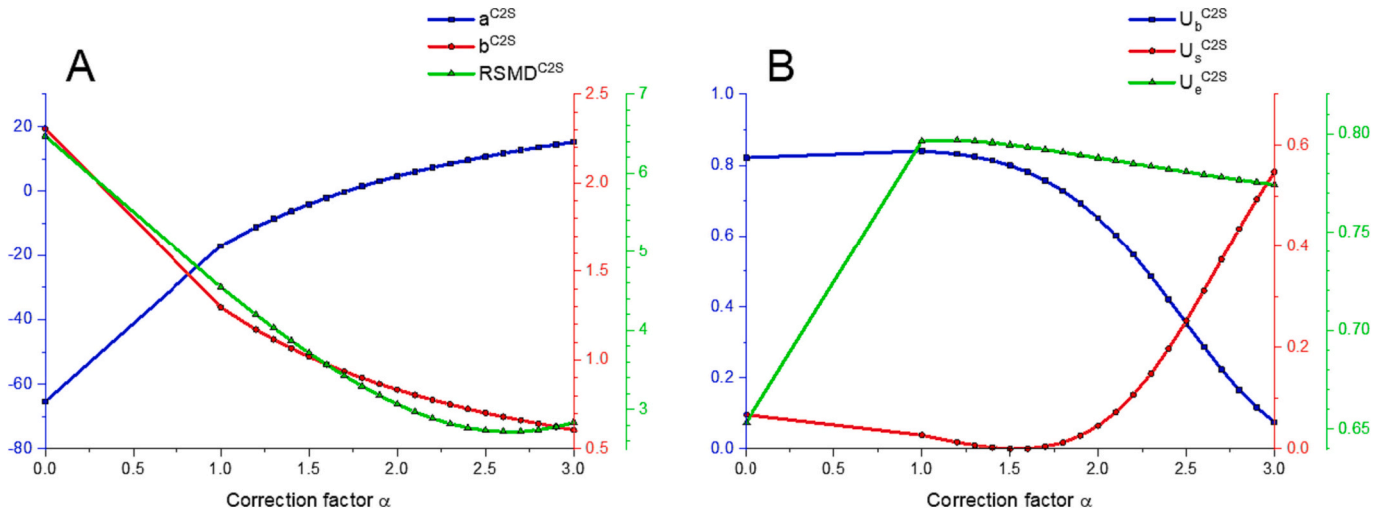

Fig. 4. A and B: Variation of the quantitative model assessment measures for a varying correction factor α.

$LOI_{Fe\text{-}corr}$. Nonetheless, the modelled C_2S content is still too high compared to the RQPA values for C_2S (Fig. 3A). Hence, a multiplication factor "α" for the $LOI_{Fe\text{-}corr}$ may be applied in order to increase the correlation with the RQPA values of C_2S:

$$X_{C_2S(total)} = 2.867\,X_S + 2.185\,X_P + 1.925\,X_V - \alpha^{*}LOI_{Fe-corr} \quad (3)$$

As the correction is applied, the amounts of modelled C_2S decrease (Fig. 3). The largest impact is visible on F-Type samples, which decrease from an initial average value of 43.5 wt% to 38.7 and 31.5 wt% at α of 1 and 2.5, respectively. In comparison, C-Type samples are less affected by this correction. The initial amounts of C_2S C-Type samples are 46.4 wt% and decrease to 45.7 and 44.8 wt% at α of 1 and 2.5, respectively. The lower decrease of C-Type samples compared to F-Type samples is caused by the significantly higher $LOI_{Fe\text{-}corr}$ of the F-Type samples (Table 8). In order to test for the correct α factor, multiple α's were tested (i.e. from 1 to 3 with a 0.1 step size). Additionally, the effect of the varying α on the quantitative model assessment measures is plotted (Fig. 4) in order to identify the ideal α for the model. The model assessment measures for the regression (a^{C2S}, b^{C2S} and U_s^{C2S}) are the best for an α at around 1.5. On the contrary, model assessment measures regarding bias (U_b^{C2S} and $RMSD^{C2S}$) are better at higher α-values (>2.3). The contrasts can be best explained by evaluating Fig. 4, where at lower α the plotted data form a

better regression (i.e. higher U_e^{C2S}), but a higher α all points move closer to the 1:1 regression, especially the F-Type samples because they have the highest $LOI_{Fe\text{-}corr}$. In our point of view, it is advised to use a lower α value around 1.5 rather than higher ones, so that the best regression values are reached despite the overestimation of C_2S. One reason for the remaining overestimation of modelled C_2S values compared to the RQPA values might also be the omission of C_3S in the Bogue BOF slag equations even though only small amounts (<2 wt%) have been detected. Another reason could be that all V_2O_5 is incorporated as C_3V into the total C_2S. It is commonly accepted that V not only incorporates into C_2S but also into the $C_2(A,F)$. However, V may occur in BOF slag in different oxidation states (V^{3+}, V^{4+} and V^{5+}) which are very sensitive to the oxygen fugacity during cooling and hence will control V distribution between $C_2(A,F)$ and C_2S [53,54,61,62]. If as in the Bogue BOF slag model $V^{5+}$is assumed, C_3V is the endmember in the total C_2S solid solution series. C_3V varies between 1.6 and 2.9 wt% in the Bogue BOF slag calculation, hence if some of the V is present as V^{3+} it would bind a certain amount of Ca and be incorporated into $C_2(A,F)$. This would have the consequence that the amount of $C_2(A,F)$ is increased and total C_2S is decreased. This effect and would reduce the overestimation of C_2S. However, since there is no information in the literature about the general or mean distribution of V between C_2S and $C_2(A,F)$ and it is known that the oxidation state of V and hence its distribution is very sensitive, it is assumed for reasons of simplicity of the Bogue BOF slag model that all the V is V^{5+} and hence incorporated as C_3V (i.e. $Ca_3V_2O_8$). Of course adjustments to this assumption are always possible based on future research results.

The correction of the RO-Phase requires a different approach compared to C_2S, because the RO-Phase is underestimated. As is suggested in Paragraph 3.2, 3 wt% of CaO are added to the RO-Phase in our model data because that is generally the amount of CaO incorporated by the RO-Phase in the BOF slags of Tata Steel plant in IJmuiden, The Netherlands [9,13]. However, the amount of CaO in the RO-Phase may vary depending on the amount MgO in the RO-Phase. Generally, the higher the amount of MgO in the RO-Phase the less CaO may be incorporated [32]. Though, for the sake of simplicity of the model it is suggested to keep the incorporated amount of CaO in the RO-Phase constant and only adjust the value if BOF slag with significant different chemical composition is modelled. For example if the BOF slag compositions of single converter heats are modelled. The addition of CaO in the RO-Phase equation results in the following equation:

$$X_{RO} = \left(\left(X_f - 0.31\,X_{Ff}\right) + X_M + X_m + X_{Cr}\right)/(1-\beta) \tag{4}$$

whereas β presents the fraction of CaO added in the RO-Phase. As a consequence of the added CaO to the RO-Phase, it is also required to adjust the Bogue BOF slag equation for f-C:

$$X_{f-C} = X_C - (\,1.867\,X_S + 1.185\,X_P + 0.925\,X_V + 1.1\,X_A + 1.404\,X_T + 1.004{*}\omega_i{*}X_{Fe\ total}) - \beta{*}X_{RO} \tag{5}$$

Fig. 5 presents the effect of the CaO correction on the RO-Phase. The CaO correction causes the amount of RO-Phase match the RQPA results better but a slight underestimation compared to the RQPA values is still present. Since we know the approximate amount of CaO in the RO-Phase, a further correction with higher CaO contents (>3 %; i.e. β > 0.03) is avoided. The usage of a higher ω_i, would have a higher impact but that would have the effect that the $C_2(A,F)$ is significantly overestimated. A further investigation about a better fitting of the ω_i is will not be performed because on the one hand this would extend this manuscript too much and on the other it would be outside of the plant reported range of the ω_i. Therefore, the final model assessment will be based on the best fitting ω_i which is 0.25.

The corrected and final Bogue BOF slag equations are presented in Equation Sequence 5 with $LOI_{Fe\text{-}corr}$ corrected C_sS and its correction factor α and the CaO corrected RO-Phase with the β-correction factor. Fig. 6 illustrates the results of the final Bogue BOF slag equations at α of 1.5, β of 0.03 and an ω_i of 0.25. The resulting total model assessment

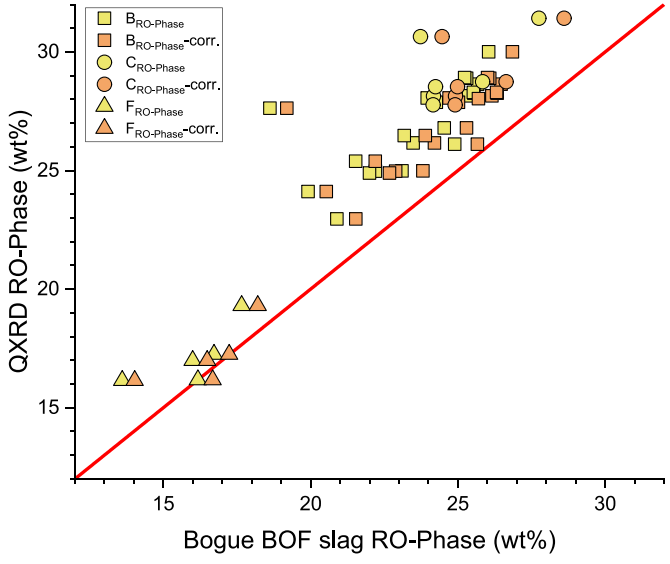

Fig. 5. Change of RO-Phase quantified by the Bogue BOF slag when a β correction factor of 0.03 (i.e. addition of CaO in the RO-Phase) is applied at a ω_i of 0.25. The red solid line presents the 1:1 regression. (For interpretation of the references to colour in this figure legend, the reader is referred to the web version of this article.)

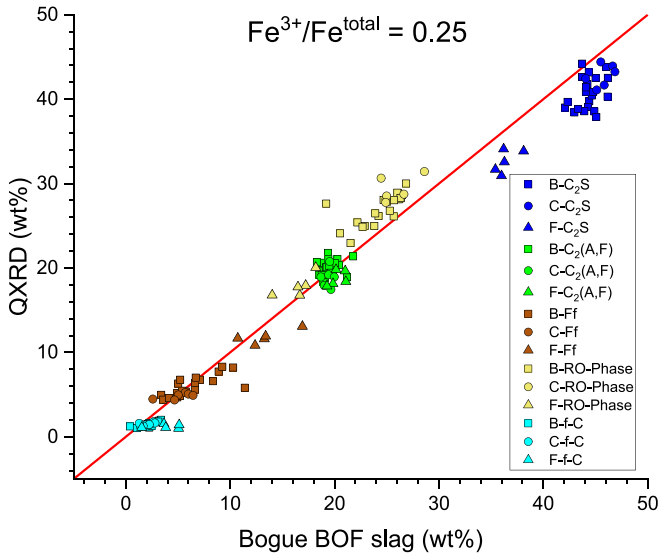

Fig. 6. Results of the computed Bogue BOF slag using Equation Sequence 5 at an ω_i of 0.25, α of 1.5 and β of 0.03 versus RQPA results. The red solid line presents the 1:1 regression. (For interpretation of the references to colour in this figure legend, the reader is referred to the web version of this article.)

measures will be compared to total model assessment measures of the classical Bogue approach applied to OPC.

$$X_{C_2S(total)} = 2.867\,X_S + 2.185\,X_P + 1.925\,X_V - \alpha^{*}LOI_{Fe-corr}$$

$$X_{C_2(A,F)} = 2.434^{*}\omega_i{}^{*}X_{Fe\ total} + 2.1\,X_A + 2.404\,X_T$$

$$X_{Ff} = 1.45^{*}(X_F - (0.587^{*}(2.434^{*}\omega_i{}^{*}X_{Fe\ total}))$$

$$X_{RO} = \left(\left(X_f - 0.31\,X_{Ff}\right) + X_M + X_m + X_{Cr}\right)/(1-\beta)$$

$$X_{f-C} = X_C - (\,1.867\,X_S + 1.185\,X_P + 0.925\,X_V + 1.1\,X_A + 1.404\,X_T + 1.004^{*}\omega_i{}^{*}X_{Fe\ total}) - \beta^{*}X_{RO}$$

Equation Sequence 5 gives the wt% of the major BOF slag phases by using the wt% of oxides (Bogue equation) with correction factors α and β for the correction of C_2S, RO-Phase and f-C, respectively.

4.5. Bogue BOF slag model validation

4.5.1. Modelled chemical phase composition

In order to validate the model, it is possible to compare the chemical composition of the modelled BOF slag phases with actual data measured by energy dispersive spectroscopy (EDS) or wavelength dispersive spectroscopy (WDS). For this case it was elected to use already published chemical composition data of phases determined with large-area phase mapping. The data that was used was determined by EDS and processed by the in-house software PARC [13]. The advantage using large area phase mapping is that it has a higher accuracy for the average chemical composition of phases compared to the traditional point and shoot approach. The used data set was also measured on average BOF slag from the same steel plant (Tata Steel IJmuiden) as in this study. It should be noted that a drawback by using EDS or WDS data is that it cannot differentiate between the different Fe species (Fe^0, Fe^{2+} and Fe^{3+}) and hence it is not possible to differentiate between Ff and the RO-Phase.

From Table 11, it can be seen that that differences in C_2S composition are small for CaO, P_2O_5 and SiO_2 (<3 wt%). Small amounts of minor oxides in C_2S like MgO, MnO, Al_2O_3 and Fe_2O_3 are below 3 wt% in the PARC compositions, whereas these oxides are not accounted for in the Bogue BOF slag model. The high amount of Cr_2O_3 in the PARC compositions of C_2S needs to be treated with care because the Cr emission spectrum in the EDS analysis overlaps with the Ca + Si Kα sum peaks, causing an overestimation of Cr_2O_3 in C_2S. The major components for $C_2(A,F)$ (i.e. CaO, Fe_2O_3 and Al_2O_3) are within a 5 wt% range. Maybe the most significant difference is that the model composition of $C_2(A,F)$ has no V_2O_5, whereas V_2O_5 values are the highest in the PARC $C_2(A,F)$ compositions (1.5 wt%). However, considering that usually much more C_2S than $C_2(A,F)$ is contained in BOF slag (usually 2:1 ratio) more V_2O_5 is contained in the C_2S than the $C_2(A,F)$. Therefore, it was decided to incorporate the total amount of V_2O_5 into the C_2S, which was also discussed in Paragraph 4.4. The assessment of the differences of the Fe-oxides Ff and RO-Phase between PARC compositions and modelled Bogue BOF slag compositions is difficult because of the above mentioned circumstances that Ff and RO-Phase are summarized as one phase in PARC [9,13,63]. However, MgO and MnO are lower in the combined PARC phase (Ff + RO-Phase) compared to the RO-Phase in the Bogue BOF slag model. This is logical because MgO and MnO are diluted in the combined PARC phase due to the addition of Ff to the RO-Phase.

To summarize, the average composition of the major BOF slag phases modelled by the Bogue approach gives only small differences to measured compositions. These small differences between the PARC compositions and the Bogue BOF slag model are the lack of V_2O_5 in the

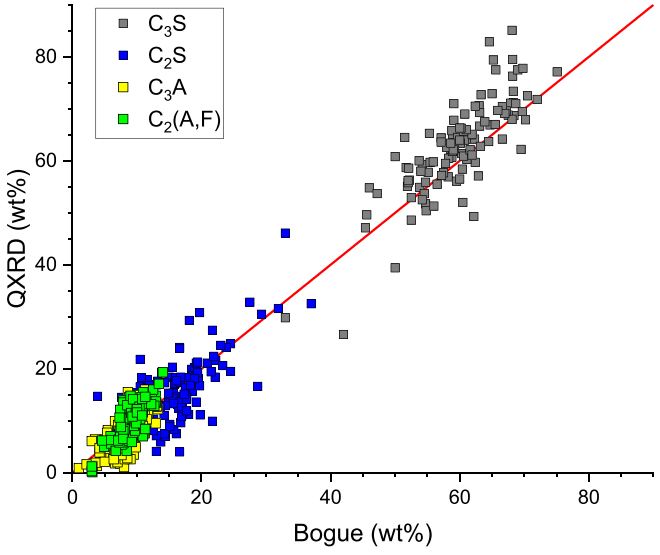

Fig. 7. Computed OPC phases determined by the using classical cement Bogue calculation versus RQPA results for the data set of [64]. The red solid line presents the 1:1 regression. (For interpretation of the references to colour in this figure legend, the reader is referred to the web version of this article.)

Table 11
Calculated mean of B-type samples chemical phase composition of phases obtained with the Bogue BOF slag model (Equation Sequence 5; ω_i of 0.25, an α of 1.5 and β of 0.03) and the determined chemical composition data from large-area phase mapping software PARC [13].

Phase compositions of the Bogue BOF slag model													
Phases	Al_2O_3	CaO	Cr_2O_3	Fe_2O_3	FeO	Met. Fe	MgO	MnO	P_2O_5	SiO_2	TiO_2	V_2O_5	Total
C_2S	0.0	63.4	0.0	0.0	0.0	0.0	0.0	0.0	3.5	30.4	0.0	2.8	100
$C_2(A,F)$	10.2	46.9	0.0	34.9	0.0	0.0	0.0	0.0	0.0	0.0	8.0	0.0	100
Ff	0.0	0.0	0.0	69.0	31.0	0.0	0.0	0.0	0.0	0.0	0.0	0.0	100
RO-Phase	0.0	3.0	1.3	0.0	42.7	0.0	34.2	18.7	0.0	0.0	0.0	0.0	100
PARC after [13]													
C_2S	0.5	61.4	1.2	2.2	n.a.	n.a.	0.3	0.1	3.4	28.2	1.2	1.1	99.6
$C_2(A,F)$	11.2	42.3	0.4	35.1	n.a.	n.a.	0.6	1.2	0.1	1.8	5.1	1.5	99.4
Ff + RO-Phase	0.2	2.5	0.5	60.3	n.a.	n.a.	23.8	11.7	0.0	0.8	0.0	0.1	99.9

Table 12
Comparison between the quantitative model assessment measures for the classical cement Bogue of the data set of [64] and the corrected Bogue BOF slag model (ω_i of 0.25, an α of 1.5 and β of 0.03).

Model	Phase	a	b	SSPE	U_b	U_s	U_e	RMSD
Bogue cement	C_3S	−3.3	1.104	4130	0.22335	0.01348	0.668	6.10
	C_2S	1.6	0.870	2759	0.85248	0.03197	0.490	4.99
	$C_2(A,F)$	−1.3	1.045	932	2.48240	0.00455	0.432	2.90
	C_3A	−2.4	1.343	683	0.22805	0.09324	0.620	2.48
	Total	−0.9	1.060	8503	0.00372	0.09102	0.969	8.75
Bogue BOF slag	C_2S	−3.8	1.006	477	0.81975	0.00002	0.794	3.92
	$C_2(A,F)$	16.4	0.166	51	0.00000	0.28305	0.015	1.28
	Ff	1.8	0.673	80	0.12355	0.46104	0.825	1.61
	RO-Phase	0.5	1.083	276	0.69259	0.01009	0.852	2.98
	Total	1.7	0.910	883	0.02349	0.20813	0.965	2.64

$C_2(A,F)$ model composition and the difficulty in assessing the differences between Ff and the RO-Phase due to the summarization of these two phases in PARC.

4.5.2. Bogue BOF slag and classical cement Bogue results in comparison

The comparison in accuracy of Bogue BOF slag and the classical cement Bogue will help to establish whether the Bogue BOF slag is a viable and reliable alternative to RQPA in order to predict the major phase quantities of BOF slag (C_2S, $C_2(A,F)$, Ff, RO-Phase and possibly f-C) for BOF slag producers and users. To be able to compare the classical cement Bogue and the here presented Bogue BOF slag model, a collected data set of Stutzmann [64] was used. The data set consists of multiple data sets where RQPA and Bogue calculations were performed on cement. To be consistent only data sets were used where a RQPA was reported, which are in total 110 data points (Fig. 7). The data set was used to calculate the model assessment measures which are compared here with the model assessment measures of the corrected Bogue BOF slag model at α of 1.5, β of 0.03 and an ω_i of 0.25.

The classical cement Bogue gives better a^{Total}, b^{Total}, U_b^{Total}, U_s^{Total} and U_e^{Total} compared to the corrected Bogue BOF slag calculation, with −0.9, 1.06, 0.0037, 0.091 and 0.969, respectively (Table 12) but the Bogue BOF slag performs comparable especially with a^{Total} b^{Total} and U_e^{Total} of 1.7 wt%, 0.91 and 0.965, respectively. It should be noted however that $RMSD^{Total}$ of Bogue BOF slag is significantly better with 2.64 compared to the classical cement Bogue with 8.75 (Table 12). To bring these number into words, the classical cement Bogue performs better in terms of correlation with the 1:1 regression line based on the lower U_s^{Total} and better b^{Total} values. However, the lower $RMSD^{Total}$ of Bogue BOF slag shows that a significantly better prediction of phase quantities is achieved with the Bogue BOF slag model compared to the classical cement Bogue. Therefore, it can be argued that the Bogue BOF slag model is performing better compared to classical cement Bogue. One reason for this is that the Bogue BOF slag model does not work with fixed composition of phases, as the composition of C_2S changes with the amounts of P_2O_5, V_2O_5 and SiO_2, RO-Phase changes with amounts of MgO, MnO and remaining FeO and $C_2(A,F)$ depends on the ω_i and the amount of Al_2O_3. In comparison, the classical cement Bogue works with fixed stoichiometric compositions (e.g. C_4A,F and C_3A), which was pointed out as the major error in the classical cement Bogue [40]. Though, $RMSD^{total}$ values are expected to increase if a larger data set for BOF slag is available with more varying compositions and different scientists would perform RQPA introducing higher variances [7,29]. This also illustrates a demand of a powder RQPA protocol for BOF slag as it is present for OPC with ATSM C 1365 [65].

4.6. Comparison of Bogue BOF slag and available literature RQPA data

Only one other research paper was found in the literature that presented RQPA data and chemical composition data determined by XRF coupled with Fe speciation determination of raw BOF slag (Table 13) [33]. The reported Fe^{2+} and Fe^{3+} values have been recalculated to FeO and Fe_2O_3. The corrected Bogue BOF slag equations were applied with a β of 0.03 on the chemical composition data. The used ω_i was 0.505, which is calculated from the reported chemical composition. Because no Ff was detected it was assumed that all Fe^{3+} is initially incorporated into $C_2(A,F)$. It should be noted that no LOI was reported, hence C_2S was not corrected. Also a correction of C_2S seems unnecessary since the used BOF slag seems to be relatively fresh, because no Cc nor CH was detected or reported. The reported RQPA values differ significantly from our Bogue BOF slag calculation. C_2S and $C_2(A,F)$ are both about 6 wt% lower in the Bogue BOF slag model compared to the reported RQPA values, whereas the RO-Phase was significantly higher (~7 wt%). Based on the reported chemical composition the Bogue BOF slag values are more realistic, because there is from a stoichiometric point of view: i) not enough SiO_2, P_2O_5 and V_2O_5 available in the reported chemical composition to form the reported amounts of >40 wt% C_2S determined by RQPA, ii) not enough Al_2O_3, Fe_2O_3 and TiO_2 available to form 38 wt % of $C_2(A,F)$ and iii) there is much more FeO, MgO and MnO available to form the RO-Phase as the reported 13 wt%. These deviations cannot be explained simply by incorporation of foreign elements into different phases. It is possible that the significant overestimation of C_2S and underestimation of the RO-Phase is due to microabsorption effects. Samples containing significant amounts of Fe (>~8 wt%) cause microabsorption during an XRD measurement with Cu as X-ray source. As a result Fe containing phases such as the RO-Phase are underestimated and non-Fe containing phases such as C_2S are overestimated [27,28,66]. Although, the underestimation would also apply to $C_2(A,F)$, $C_2(A,F)$ is according to the Bogue BOF slag calculation overestimated by

Table 13
Chemical composition, phase composition by RQPA as reported by [33], FeO and Fe_2O_3 were recalculated from the reported Fe^{2+} and Fe^{3+}. The phase composition based on the Bogue BOF slag model was calculated with an ω_i of 0.505, and α of 0 and β of 0.03.

	Al_2O_3	CaO	Cr_2O_3	Fe_2O_3	FeO	Met. Fe	MgO	MnO	P_2O_5	SiO_2	TiO_2	V_2O_5	Fe total
Chemical Composition	2.10	44.50	n.r.	14.87	13.12	n.r.	2.20	4.80	2.00	10.10	0.90	0.40	20.6

	C_2S	$C_2(A,F)$	Ff	RO-Phase	f-C	amorphous
RQPA	40.6	38	0	13	5.7	2.7
Bogue BOF slag	34.1	31.9	0	20.7	8.3	

RQPA. This might be due to the sensitivity of the $C_2(A,F)$ stoichiometry and the related intensities in the XRD pattern. If a different stoichiometry for the $C_2(A,F)$ is applied in the Rietveld RQPA than the real $C_2(A,F)$ stoichiometry it has significant influence on the quantified amounts of $C_2(A,F)$ [4].

5. Conclusions

This study presents a method to calculate the main phases of BOF slag (C_2S, $C_2(A,F)$, Ff, RO-Phase and f-C only based on the chemical composition determined by XRF and Fe redox titration. The modelling approach applied to calculate BOF slag phase quantities was comparable to the classical cement Bogue approach. The chemical composition of 32 BOF slag samples was determined and the phase quantities of the main phase of BOF slag were calculated. Four calculations were performed based on different ω_i (i.e. initial Fe^{3+}/Fe^{total} of 0.25, 0.292, 0.33 and a variable ω_i depending on the amount of Fe^{total}) that is initially incorporated into $C_2(A,F)$. The results of the four calculations were compared to the RQPA values by using a quantitative model assessment approach.

The results show that the Bogue BOF slag model gives the best model assessment values at an ω_i of 0.25. Moreover, C_2S quantities and model assessment measures do not change by changing the ω_i, but are significantly overestimated. Therefore, a correction α is applied based on $LOI_{Fe\text{-}corr}$. Also a correction factor for the RO-Phase was applied (β), based on additional CaO that can be incorporated. It is recommended to use Equation Sequence 5 with an ω_i of 0.25, an α of 1.5 and β of 0.03 but other values can be used depending on the BOF slag properties. The authors would like to emphasize here that if the Bogue BOF slag model is applied, the ω_i, α and β values should be reported too.

Two different approaches were used in order to validate the Bogue BOF slag model. The first approach compared the derived average phase compositions with large-area phase compositions determined by PARC from EDS data. Only small differences were found between the measured compositions and the modelled phase compositions, which related to the lack of minor oxides. In the second approach, an extensive literature data set for OPC with RQPA and classical cement bogue of [64] was used to calculate the quantitative model assessment measures and compare them to the results of the Bogue BOF slag model. It was shown that the Bogue BOF slag model gives comparable values to the classical cement Bogue for the quantitative model assessment measures. Moreover, the Bogue BOF slag model was applied to one literature data set of BOF slag, which contained chemical composition, Fe speciation and RQPA. It was found that Bogue BOF slag model phase quantities were significantly deviating from RQPA values, whereas the Bogue BOF slag model gives more realistic phase quantities than the RQPA simply by evaluating chemical composition.

Although, the Bogue BOF slag model overestimates the amount of C_2S and Fe speciation determination is required, the Bogue BOF slag model presents a viable method to quantify the phases of BOF slag based on the chemical composition. The Bogue BOF slag model is much quicker and more reliable to perform than a quantitative Rietveld phase analysis. Moreover, the model is very simple to apply and requires no difficult calculations. The presented model allows the validation of RQPA results for BOF slag. Hence, it has a viable future for BOF slag produces and users.

Future adjustments that would probably improve the Bogue BOF slag model are: i) partial incorporation of V_2O_5 into the $C_2(A,F)$, ii) usage of different ω_i, especially a variable one that is based on the Fe^{total} and iii) if the f-C is amount is predetermined it is possible to derive C_2S and C_3S independently, as it is performed in the classical cement Bogue.

CRediT authorship contribution statement

J.C.O. Zepper: Conceptualization, Methodology, Validation, Formal analysis, Investigation, Writing – original draft, Visualization. **S.R. van der Laan:** Conceptualization, Resources, Supervision, Project administration. **K. Schollbach:** Conceptualization, Writing – review & editing, Supervision. **H.J.H. Brouwers:** Conceptualization, Methodology, Resources, Writing – review & editing, Supervision, Funding acquisition.

Declaration of competing interest

The authors declare the following financial interests/personal relationships which may be considered as potential competing interests: J. C.O. Zepper reports financial support was provided by M2i Materials Innovation Institute. J.C.O. Zepper reports financial support was provided by Netherlands Foundation of Scientific Research Institutes. J.C.O. Zepper reports equipment, drugs, or supplies were provided by Tata Steel Netherlands.

Data availability

Data will be made available on request.

Acknowledgements

The authors would like to express their gratitude for the financial support of the Nederlandse Organisatie voor Wetenschappelijk Onderzoek (NWO) by funding this research (project no.10023338) and Materials Innovation Institute (M2i) for managing this project. Also the authors want to thank Rick Willemse for sampling the representative samples. Acknowledged is also the work of staff of the analytical labs of Tata Steel IJmuiden, who helped carrying out the sample preparation and analytical work of samples. Additionally, Mary Wijngaarden-Kroft and Richard Kos are thanked who helped with the sample preparation and analyzing the XRD samples. Not forgotten should be the work of Stefan Melzer who gave important advice for a reliable Rietveld quantitative phase analysis.

Appendix A. Appendix text

7 different measures for the model assessment

- a refers to the value where the linear regression line intercepts the y-axis.
- b refers to the slope value of the linear regression.
- SSPE refers to the squared sum of the predictive error. It is an absolute value how much the predicted data deviates from the modelled data on an average basis.
- U_b is a measure to assess how much the means between predicted and observed value differ from each other and therefore expresses whether there is a bias in the modelled data. This expression is different to RMSD and SSPE because it assesses whether the observed data deviates from the 1:1 regression.
- U_s is a measure to assess how much the slope of the modelled regression line is associated with the 1:1 regression line.
- U_e is also known as R^2 and measures how much the predicted data is aligned with the observed data.

- RMSD refers to the root mean squared deviation and presents a measure how much the predicted values deviate from the observed values in the form of the same units.

Table Appendix 1
Results of the Bogue BOF slag model an ω_i of 0.25, α of 0 and β of 0.

$\omega_i = 0.25$							
Sample ID	C_2S	$C_2(A,F)$	Ff	RO-Phase	Met. Fe	f-C	Total
B1	47.2	18.8	10.3	19.9	1.0	2.9	100.0
B2	47.4	18.3	7.1	22.2	1.1	3.8	100.0
B3	45.9	19.4	8.9	21.5	1.3	3.0	100.0
B4	46.7	18.9	8.4	22.0	1.1	2.9	100.0
B5	45.3	19.8	9.3	20.9	1.9	2.8	100.0
B6	46.5	19.4	3.4	25.7	1.9	3.1	100.0
B7	45.5	19.7	5.7	24.9	1.1	3.0	100.0
B8	44.8	21.8	4.9	26.0	1.2	1.2	100.0
B9	45.3	19.9	6.6	24.5	0.7	2.9	100.0
B10	46.0	20.3	4.9	25.4	1.2	2.2	100.0
B11	44.8	20.4	5.2	25.5	1.2	2.9	100.0
B12	43.6	21.2	6.6	25.3	1.4	1.8	100.0
B13	45.8	19.2	6.6	23.1	1.4	3.9	100.0
B14	46.6	18.5	3.6	25.2	1.8	4.2	100.0
B15	47.1	18.8	4.1	25.5	1.1	3.3	100.0
B16	46.6	19.1	5.4	23.5	2.2	3.2	100.0
B17	45.7	19.2	6.6	23.2	1.6	3.6	100.0
B18	44.7	20.0	11.4	18.6	2.6	2.7	100.0
B19	45.7	19.5	6.7	24.0	1.1	3.1	100.0
B20	45.9	18.9	5.0	24.3	2.0	3.9	100.0
B21	46.1	19.6	5.2	24.9	1.5	2.6	100.0
C15	46.7	19.5	5.7	24.2	1.7	2.1	100.0
C16	47.3	18.7	5.0	24.2	1.3	3.4	100.0
C17	46.1	19.0	6.0	24.2	1.2	3.5	100.0
C18	45.8	19.4	4.7	25.8	1.2	3.0	100.0
C19	45.4	20.0	2.6	27.7	1.8	2.5	100.0
C21	47.0	19.7	6.4	23.7	1.2	2.0	100.0
F16	43.6	20.1	12.4	16.7	3.0	4.2	100.0
F17	43.6	19.8	13.3	16.2	1.6	5.6	100.0
F18	44.3	21.1	10.7	17.7	4.1	2.1	100.0
F19	42.3	21.0	16.9	13.6	2.0	4.2	100.0
F20	43.5	19.3	13.4	16.0	2.2	5.6	100.0

Table Appendix 2
Results of the Bogue BOF slag model an ω_i of 0.292, α of 0 and β of 0.

$\omega_i = 0.292$							
Sample ID	C_2S	$C_2(A,F)$	Ff	RO-Phase	Met. Fe	f-C	Total
B1	47.2	20.6	8.7	20.4	1.0	2.1	100.0
B2	47.4	20.2	5.5	22.7	1.1	3.1	100.0
B3	45.9	21.4	7.2	22.1	1.3	2.2	100.0
B4	46.7	20.9	6.7	22.5	1.1	2.1	100.0
B5	45.3	21.8	7.5	21.4	1.9	2.0	100.0
B6	46.5	21.4	1.7	26.2	1.9	2.2	100.0
B7	45.5	21.7	4.0	25.4	1.1	2.2	100.0
B8	44.8	23.9	3.2	26.6	1.2	0.3	100.0
B9	45.3	21.9	4.9	25.1	0.7	2.1	100.0
B10	46.0	22.3	3.2	25.9	1.2	1.4	100.0
B11	44.8	22.3	3.5	26.1	1.2	2.1	100.0
B12	43.6	23.3	4.8	25.9	1.4	1.0	100.0
B13	45.8	21.0	5.1	23.6	1.4	3.2	100.0
B14	46.6	20.4	2.0	25.7	1.8	3.4	100.0
B15	47.1	20.6	2.6	26.0	1.1	2.6	100.0
B16	46.6	21.0	3.8	24.0	2.2	2.4	100.0
B17	45.7	21.2	5.0	23.7	1.6	2.8	100.0
B18	44.7	22.1	9.7	19.2	2.6	1.8	100.0
B19	45.7	21.4	5.1	24.5	1.1	2.3	100.0
B20	45.9	20.9	3.4	24.8	2.0	3.1	100.0
B21	46.1	21.6	3.6	25.4	1.5	1.8	100.0
C15	46.7	21.5	4.0	24.7	1.7	1.3	100.0
C16	47.3	20.5	3.5	24.7	1.3	2.7	100.0
C17	46.1	20.9	4.4	24.7	1.2	2.8	100.0
C18	45.8	21.4	3.0	26.4	1.2	2.2	100.0
C19	45.4	22.0	0.9	28.3	1.8	1.7	100.0
C21	47.0	21.5	4.8	24.2	1.2	1.2	100.0

(*continued on next page*)

Table Appendix 2 (*continued*)

$\omega_i = 0.292$							
Sample ID	C_2S	$C_2(A,F)$	Ff	RO-Phase	Met. Fe	f-C	Total
F16	43.6	22.1	10.7	17.2	3.0	3.4	100.0
F17	43.6	21.7	11.7	16.7	1.6	4.8	100.0
F18	44.3	23.2	8.9	18.2	4.1	1.2	100.0
F19	42.3	23.0	15.2	14.1	2.0	3.4	100.0
F20	43.5	21.2	11.8	16.5	2.2	4.8	100.0

Table Appendix 3
Results of the Bogue BOF slag model an ω_i of 0.33, α of 0 and β of 0.

$\omega_i = 0.33$							
Sample ID	C_2S	$C_2(A,F)$	Ff	RO-Phase	Met. Fe	f-C	Total
B1	47.2	22.3	7.2	20.9	1.0	1.4	100.0
B2	47.4	21.8	4.1	23.1	1.1	2.4	100.0
B3	45.9	23.2	5.7	22.5	1.3	1.4	100.0
B4	46.7	22.7	5.1	23.0	1.1	1.4	100.0
B5	45.3	23.7	6.0	21.9	1.9	1.2	100.0
B6	46.5	23.1	0.2	26.7	1.9	1.5	100.0
B7	45.5	23.5	2.5	25.9	1.1	1.5	100.0
B8	44.8	25.8	1.5	27.1	1.2	−0.4	100.0
B9	45.3	23.7	3.4	25.5	0.7	1.3	100.0
B10	46.0	24.1	1.7	26.4	1.2	0.7	100.0
B11	44.8	24.1	2.0	26.5	1.2	1.4	100.0
B12	43.6	25.2	3.2	26.4	1.4	0.2	100.0
B13	45.8	22.6	3.7	24.0	1.4	2.5	100.0
B14	46.6	22.0	0.6	26.2	1.8	2.7	100.0
B15	47.1	22.3	1.1	26.5	1.1	1.9	100.0
B16	46.6	22.7	2.3	24.4	2.2	1.7	100.0
B17	45.7	22.9	3.6	24.1	1.6	2.1	100.0
B18	44.7	24.0	8.1	19.6	2.6	1.1	100.0
B19	45.7	23.2	3.6	24.9	1.1	1.5	100.0
B20	45.9	22.6	1.9	25.2	2.0	2.3	100.0
B21	46.1	23.3	2.1	25.9	1.5	1.1	100.0
C15	46.7	23.3	2.5	25.2	1.7	0.6	100.0
C16	47.3	22.1	2.1	25.1	1.3	2.0	100.0
C17	46.1	22.6	2.9	25.1	1.2	2.1	100.0
C18	45.8	23.1	1.5	26.8	1.2	1.5	100.0
C19	45.4	23.8	−0.7	28.8	1.8	0.9	100.0
C21	47.0	23.2	3.4	24.7	1.2	0.5	100.0
F16	43.6	23.9	9.1	17.7	3.0	2.6	100.0
F17	43.6	23.3	10.3	17.1	1.6	4.1	100.0
F18	44.3	25.2	7.2	18.7	4.1	0.4	100.0
F19	42.3	24.9	13.6	14.6	2.0	2.7	100.0
F20	43.5	22.9	10.3	16.9	2.2	4.1	100.0

Table Appendix 4
Results of the Bogue BOF slag model an ω_i, which was variable according to Eq. (1), α of 0 and β of 0.

ω_i = variable							
Sample ID	C_2S	$C_2(A,F)$	Ff	RO-Phase	Met. Fe	f-C	Total
B1	47.2	19.6	9.6	20.1	1.0	2.5	100.0
B2	47.4	18.8	6.7	22.3	1.1	3.6	100.0
B3	45.9	21.5	7.1	22.1	1.3	2.1	100.0
B4	46.7	20.8	6.7	22.5	1.1	2.1	100.0
B5	45.3	22.0	7.4	21.5	1.9	1.9	100.0
B6	46.5	21.0	2.1	26.1	1.9	2.4	100.0
B7	45.5	21.9	3.9	25.5	1.1	2.1	100.0
B8	44.8	25.0	2.2	26.9	1.2	−0.1	100.0
B9	45.3	22.2	4.6	25.1	0.7	1.9	100.0
B10	46.0	22.3	3.2	25.9	1.2	1.4	100.0
B11	44.8	21.9	3.9	26.0	1.2	2.3	100.0
B12	43.6	24.6	3.7	26.2	1.4	0.4	100.0
B13	45.8	19.4	6.4	23.2	1.4	3.8	100.0
B14	46.6	18.9	3.3	25.3	1.8	4.0	100.0
B15	47.1	19.2	3.7	25.6	1.1	3.1	100.0
B16	46.6	20.1	4.6	23.7	2.2	2.8	100.0
B17	45.7	20.3	5.7	23.5	1.6	3.2	100.0

(*continued on next page*)

Table Appendix 4 (*continued*)

ω_i = variable							
Sample ID	C_2S	$C_2(A,F)$	Ff	RO-Phase	Met. Fe	f-C	Total
B18	44.7	22.8	9.1	19.3	2.6	1.5	100.0
B19	45.7	20.8	5.6	24.3	1.1	2.5	100.0
B20	45.9	20.4	3.8	24.7	2.0	3.3	100.0
B21	46.1	20.9	4.1	25.3	1.5	2.1	100.0
C15	46.7	21.1	4.4	24.6	1.7	1.5	100.0
C16	47.3	18.7	5.0	24.2	1.3	3.4	100.0
C17	46.1	19.7	5.4	24.3	1.2	3.3	100.0
C18	45.8	20.9	3.5	26.2	1.2	2.5	100.0
C19	45.4	22.3	0.6	28.4	1.8	1.6	100.0
C21	47.0	20.4	5.8	23.9	1.2	1.7	100.0
F16	43.6	22.3	10.6	17.3	3.0	3.3	100.0
F17	43.6	20.1	13.0	16.2	1.6	5.5	100.0
F18	44.3	25.2	7.2	18.7	4.1	0.4	100.0
F19	42.3	23.4	14.9	14.2	2.0	3.3	100.0
F20	43.5	20.1	12.7	16.2	2.2	5.3	100.0

Table Appendix 5
Results of the Bogue BOF slag model an ω_i of 0.25, α of 1.5 and β of 0.03.

$\omega_{i\ i}$ = 0.25							
Sample ID	C_2S	$C_2(A,F)$	Ff	RO-Phase	Met. Fe	f-C	Total
B1	46.1	18.8	10.3	20.5	1.0	2.2	99.0
B2	46.0	18.3	7.1	22.9	1.1	3.2	98.6
B3	44.4	19.4	8.9	22.2	1.3	2.3	98.5
B4	44.6	18.9	8.4	22.7	1.1	2.2	97.9
B5	43.0	19.8	9.3	21.5	1.9	2.2	97.7
B6	44.7	19.4	3.4	26.5	1.9	2.3	98.2
B7	44.3	19.7	5.7	25.7	1.1	2.3	98.8
B8	43.9	21.8	4.9	26.9	1.2	0.4	99.1
B9	44.9	19.9	6.6	25.3	0.7	2.1	99.5
B10	45.1	20.3	4.9	26.2	1.2	1.5	99.1
B11	43.3	20.4	5.2	26.3	1.2	2.1	98.6
B12	42.1	21.2	6.6	26.1	1.4	1.1	98.5
B13	44.2	19.2	6.6	23.8	1.4	3.2	98.5
B14	45.0	18.5	3.6	26.0	1.8	3.4	98.3
B15	46.2	18.8	4.1	26.3	1.1	2.5	99.0
B16	44.1	19.1	5.4	24.2	2.2	2.5	97.5
B17	43.7	19.2	6.6	23.9	1.6	2.9	98.0
B18	42.3	20.0	11.4	19.2	2.6	2.1	97.6
B19	44.1	19.5	6.7	24.7	1.1	2.3	98.4
B20	43.7	18.9	5.0	25.0	2.0	3.1	97.8
B21	44.3	19.6	5.2	25.7	1.5	1.8	98.2
C15	45.8	19.5	5.7	24.9	1.7	1.4	99.1
C16	46.6	18.7	5.0	25.0	1.3	2.6	99.3
C17	45.5	19.0	6.0	24.9	1.2	2.8	99.4
C18	45.1	19.4	4.7	26.6	1.2	2.2	99.3
C19	44.1	20.0	2.6	28.6	1.8	1.7	98.7
C21	46.9	19.7	6.4	24.5	1.2	1.3	99.9
F16	38.1	20.1	12.4	17.2	3.0	3.7	94.5
F17	36.3	19.8	13.3	16.7	1.6	5.1	92.7
F18	36.0	21.1	10.7	18.2	4.1	1.5	91.7
F19	35.4	21.0	16.9	14.0	2.0	3.8	93.1
F20	36.2	19.3	13.4	16.5	2.2	5.1	92.6

Phase	Initial Set Fe^{3+}/Fe^{total}	a	b	SSPE	U_b	U_s	U_e	RMSD
C_2S	0.25	-65.4	2.308	1298	0.82142	0.06730	0.653	6.47
	0.292	-65.4	2.308	1298	0.82142	0.06730	0.653	6.47
	0.33	-65.4	2.308	1298	0.82142	0.06730	0.653	6.47
	vaiable	-65.4	2.308	1298	0.82142	0.06730	0.653	6.47
$C_2(A,F)$	0.25	16.4	0.166	**51**	**0.00000**	0.28305	0.015	**1.28**
	0.292	15.9	0.171	174	0.69762	0.09548	0.019	2.37
	0.33	**15.6**	**0.173**	496	0.88894	**0.03860**	0.023	4.00
	vaiable	17.0	0.126	184	0.42899	0.37847	**0.039**	2.43
Ff	0.25	**1.8**	0.673	**80**	**0.12355**	0.46104	**0.825**	**1.61**
	0.292	2.9	0.675	109	0.35654	0.33400	0.823	1.88
	0.33	3.9	**0.676**	287	0.75558	**0.12535**	0.821	3.04
	vaiable	2.8	0.653	107	0.18150	0.38070	0.755	1.86
RO-Phase	0.25	0.5	**1.116**	404	0.78412	**0.01273**	0.852	3.61
	0.292	-0.1	1.117	308	0.71778	0.01693	**0.853**	3.15
	0.33	-0.6	1.118	**237**	**0.63282**	0.02225	**0.853**	**2.76**
	vaiable	**-0.1**	1.121	326	0.73086	0.01686	0.852	3.24
f-C	0.25	**1.1**	0.076	120	0.78042	**0.20218**	0.073	1.97
	0.292	1.3	0.078	53	0.49069	0.47074	0.081	1.31
	0.33	1.3	**0.080**	**29**	**0.03471**	0.89504	**0.086**	**0.97**
	vaiable	1.6	-0.056	78	0.46548	0.68156	0.063	1.58
Total	0.25	**2.8**	**0.847**	**1832**	**0.04431**	0.32169	0.940	**3.80**
	0.292	3.1	0.829	1890	0.06739	0.41405	**0.949**	3.86
	0.33	3.6	0.803	2318	0.07680	0.47404	0.946	4.27
	vaiable	4.7	0.790	5411	0.00018	**0.19411**	0.768	6.53

Figure Appendix 1. Modelled correlation between the lowest and highest Fe^{total}, which set the X-values. Y-values are set at 0.25 and 0.33 ω_i, respectively. The resulting regression (red solid line) determines Eq. (1).

References

[1] R.H. Bogue, Calculation of the compounds in Portland cement, Ind. Eng. Chem. 1 (1929) 192–197.

[2] P.C. Hewlett, M. Liska, P.-C. Aïtcin, J.J. Beaudoin, J. Bensted, J.S.J. van Deventer, et al., Lea's Chemistry of Cement and Concrete 5th ed., vol. 58, Butterworth-Heinemann, Oxford, 2019.

[3] R. Snellings, A. Bazzoni, K. Scrivener, The existence of amorphous phase in Portland cements: physical factors affecting Rietveld quantitative phase analysis, Cem. Concr. Res. 59 (2014) 139–146, https://doi.org/10.1016/j.cemconres.2014.03.002.

[4] M.A.T.M. Broekmans, H. Pöllmann, Reviews in Mineralogy and Geochemistry Applied Mineralogy of Cement & Concrete vol. 74, The Mineralogical Society of America, Chantilly, Virginia (US), 2012, https://doi.org/10.2138/am.2014.622.

[5] J. Skibsted, C. Hall, Characterization of cement minerals, cements and their reaction products at the atomic and nano scale, Cem. Concr. Res. 38 (2008) 205–225, https://doi.org/10.1016/j.cemconres.2007.09.010.

[6] K.L. Scrivener, A. Nonat, Hydration of cementitious materials, present and future, Cem. Concr. Res. 41 (2011) 651–665, https://doi.org/10.1016/j.cemconres.2011.03.026.

[7] L. León-Reina, A.G. De La Torre, J.M. Porras-Vázquez, G.I. Gattouso, M. Cruz, L. M. Ordonez, X. Alcobé, et al., Round robin on Rietveld quantitative phase analysis of Portland cements, J. Appl. Crystallogr. 42 (2009) 906–916, https://doi.org/10.1107/S0021889809028374.

[8] E. Benhelal, E. Shamsaei, M.I. Rashid, Challenges against CO2 abatement strategies in cement industry: a review, J. Environ. Sci. 104 (2021) 84–101, https://doi.org/10.1016/j.jes.2020.11.020.

[9] A.M. Kaja, K. Schollbach, S. Melzer, S.R. van der Laan, H.J.H. Brouwers, Q. Yu, Hydration of potassium citrate-activated BOF slag, Cem. Concr. Res. 140 (2021) 1–11, https://doi.org/10.1016/j.cemconres.2020.106291.

[10] A.C.P. Martins, J.M. Franco de Carvalho, L.C.B. Costa, H.D. Andrade, T.V. de Melo, J.C.L. Ribeiro, et al., Steel slags in cement-based composites: an ultimate review on characterization, applications and performance, Constr. Build. Mater. 291 (2021), 123265, https://doi.org/10.1016/j.conbuildmat.2021.123265.

[11] W. Franco Santos, K. Schollbach, S. Melzer, Laan S.R. Van Der, H.J.H. Brouwers, Quantitative analysis and phase assemblage of basic oxygen furnace slag hydration, J. Hazard. Mater. (2023) 450, https://doi.org/10.1016/j.jhazmat.2023.131029.

[12] World Steel Association, Steel Statistical Yearbook 2020 Extended Version, Belgium, Brussels, 2020.

[13] H. Pöllmann, Industrial Waste, 1st ed., de Gruyter, Berlin, Germany, 2021 https://doi.org/10.1515/9783110674941.

[14] H. Preßlinger, M. Mayr, R. Apfolterer, Quantitative phase evaluation of converter slags, Steel Res. 70 (1999) 209–214, https://doi.org/10.1002/srin.199905628.

[15] K. Schollbach, M.J. Ahmed, S.R. van der Laan, The mineralogy of air granulated converter slag, Int. J. Ceram. Eng. Sci. (2020) 1–16, https://doi.org/10.1002/ces2.10074.

[16] Y. Jiang, T.C. Ling, C. Shi, S.Y. Pan, Characteristics of steel slags and their use in cement and concrete—a review, Resour. Conserv. Recycl. 136 (2018) 187–197, https://doi.org/10.1016/j.resconrec.2018.04.023.

[17] M.J. Ahmed, W.F. Santos, H.J.H. Brouwers, Air granulated basic Oxygen furnace (BOF) slag application as a binder : effect on strength, volumetric stability, hydration study, and environmental risk, Constr. Build. Mater. (2023) 367, https://doi.org/10.1016/j.conbuildmat.2023.130342.

[18] E. Belhadj, C. Diliberto, A. Lecomte, Properties of hydraulic paste of basic oxygen furnace slag, Cem. Concr. Compos. 45 (2014) 15–21, https://doi.org/10.1016/j.cemconcomp.2013.09.016.

[19] E. Belhadj, C. Diliberto, A. Lecomte, Characterization and activation of basic oxygen furnace slag, Cem. Concr. Compos. 34 (2012) 34–40, https://doi.org/10.1016/j.cemconcomp.2011.08.012.

[20] A.M. Kaja, S. Melzer, H.J.H. Brouwers, Q. Yu, On the optimization of BOF slag hydration kinetics, Cem. Concr. Compos. 124 (2021), 104262, https://doi.org/10.1016/j.cemconcomp.2021.104262.

[21] J. Sun, Z. Chen, Effect of silicate modulus of water glass on the hydration of alkali-activated converter steel slag, J. Therm. Anal. Calorim. 138 (2019) 47–56, https://doi.org/10.1007/s10973-019-08146-3.

[22] J. Sun, Z. Zhang, S. Zhuang, W. He, Hydration properties and microstructure characteristics of alkali – activated steel slag, Constr. Build. Mater. 241 (2020) 118–141, https://doi.org/10.1016/j.conbuildmat.2020.118141.

[23] D. Wang, J. Chang, W.S. Ansari, The effects of carbonation and hydration on the mineralogy and microstructure of basic oxygen furnace slag products, J. CO2 Util. 34 (2019) 87–98, https://doi.org/10.1016/j.jcou.2019.06.001.

[24] F. Engström, D. Adolfsson, Q. Yang, C. Samuelsson, B. Bjo, Crystallization behaviour of some steelmaking slags, Steel Res. Int. (2010) 81, https://doi.org/10.1002/srin.200900154.

[25] M. Tossavainen, F. Engstrom, Q. Yang, N. Menad, Characteristics of steel slag under different cooling conditions, Waste Manag. 27 (2007) 1335–1344, https://doi.org/10.1016/j.wasman.2006.08.002.

[26] J. Waligora, D. Bulteel, P. Degrugilliers, D. Damidot, J.L. Potdevin, M. Measson, Chemical and mineralogical characterizations of LD converter steel slags: a multi-analytical techniques approach, Mater. Charact. 61 (2010) 39–48, https://doi.org/10.1016/j.matchar.2009.10.004.

[27] B.D. Cullity, S.R. Stock, Elements of X-ray Diffraction, Second edition, Addison-Wesley Publishing Company, Inc, Notre Dame, Indiana, USA, 1978.
[28] Y.M. Mos, A.C. Vermeulen, C.J.N. Buisman, J. Weijma, X-ray diffraction of iron containing samples: the importance of a suitable configuration, Geomicrobiol J. 35 (2018) 511–517, https://doi.org/10.1080/01490451.2017.1401183.
[29] N.V.Y. Scarlett, I.C. Madsen, L.M.D. Cranswick, T. Lwin, E. Groleau, G. Stephenson, et al., Outcomes of the International Union of Crystallography Commission on Powder Diffraction round robin on quantitative phase analysis: samples 2, 3, 4, synthetic bauxite, natural granodiorite and pharmaceuticals, J. Appl. Crystallogr. 35 (2002) 383–400, https://doi.org/10.1107/S0021889802008798.
[30] J.C.O. Zepper, K. Schollbach, S.R. van der Laan, H.J.H. Brouwers, Quality assurance of processed BOF slag: a case study, in: 8th Int. Slag Valoris. Symp, KU Leuven, Mechelen, Begium, 2023, pp. 86–90.
[31] S. Ashrit, P.K. Banerjee, U.G. Nair, V. Rayasam, Thermogravimetric analysis of LD slag waste fines in the range of 0-6 mm and establishing the correlation between free lime and weight loss of LD slag fines, Metall. Res. Technol. (2017) 114, https://doi.org/10.1051/metal/2017023.
[32] M. Gautier, J. Poirier, F. Bodénan, G. Franceschini, E. Véron, Processing basic oxygen furnace (BOF) slag cooling : laboratory characteristics and prediction calculations, Int. J. Miner. Process. 123 (2013) 94–101, https://doi.org/10.1016/j.minpro.2013.05.002.
[33] C. Liu, S. Huang, B. Blanpain, M. Guo, Effect of Al2O3 addition on mineralogical modification and crystallization kinetics of a high basicity BOF steel slag, Metall. Mater. Trans. B Process Metall. Mater. Process. Sci. 50 (2019) 271–281, https://doi.org/10.1007/s11663-018-1465-7.
[34] H.P. Klug, L.E. Alexander, X- Ray Diffraction Procedures for Polyerystalline and Amorphous Materials, 2nd ed., John Wiley & Sons, New York, 1974.
[35] C. van Hoek, J. Small, S. van der Laan, Large-area phase mapping using PhAse Recognition and Characterization (PARC) software, Micros Today 24 (2016) 12–21, https://doi.org/10.1017/s1551929516000572.
[36] L. Jiang, Y. Bao, Q. Yang, Ã.Y. Chen, Ã.G. Liu, F. Han, et al., Formation of spinel phases in oxidized BOF slag under different cooling conditions, Steel Res. Int. 88 (2017) 9–13, https://doi.org/10.1002/srin.201700066.
[37] M. Jawad Ahmed, K. Schollbach, S. van der Laan, M. Florea, H.J.H. Brouwers, A quantitative analysis of dicalcium silicate synthesized via different sol-gel methods, Mater. Des. 213 (2022), 110329, https://doi.org/10.1016/j.matdes.2021.110329.
[38] Standard Specification for Partland Cement, ASTM C150-09. Annu. B. ASTM Stand vol. 4.01, ASTM International, West Conshoohocken, PA, 2010, pp. 1–6.
[39] H.J.H. Brouwers, A Hydration Model of Portland Cement Using the Work of Powers and Brownyard, SN3039 ed., Eindhoven University of Technology/Portland Cement Association, Skokie, Illinois, U.S., 2011.
[40] H.F.W. Taylor, Cem. Chem. 20 (1998) 9465.
[41] K. Schollbach, Laan S. Van Der, Long term weathering of converter slag, in: ICSBM 2019 – 2nd Int. Conf. Sustain. Build. Mater, 2019, pp. 1–10.
[42] S.K. Singh, P. Rekha, M. Surya, Utilization of Linz–Donawitz slag from steel industry for waste minimization, J. Mater. Cycles Waste Manag. 22 (2020) 611–627, https://doi.org/10.1007/s10163-020-00981-z.
[43] P.Y. Mahieux, J.E. Aubert, G. Escadeillas, M. Measson, Quantification of hydraulic phase contained in a basic oxygen furnace slag, J. Mater. Civ. Eng. 26 (2014) 593–598, https://doi.org/10.1061/(asce)mt.1943-5533.0000867.
[44] Y. Lan, pei, Liu Q cai, Meng F, Niu D liang, Zhao H., Optimization of magnetic separation process for iron recovery from steel slag, J. Iron Steel Res. Int. 24 (2017) 165–170, https://doi.org/10.1016/S1006-706X(17)30023-7.
[45] S. Wang, C. Wang, Q. Wang, Z. Liu, W. Qian, C.Z. Jin, et al., Study on cementitious properties and hydration characteristics of steel slag, Pol. J. Environ. Stud. 27 (2018) 357–364, https://doi.org/10.15244/pjoes/74133.
[46] Y. Xue, S. Wu, H. Hou, J. Zha, Experimental investigation of basic oxygen furnace slag used as aggregate in asphalt mixture, J. Hazard. Mater. 138 (2006) 261–268, https://doi.org/10.1016/j.jhazmat.2006.02.073.
[47] Z. Xu, J. Hwang, R. Greenlund, X. Huang, J. Luo, S. Anschuetz, Quantitative determination of metallic iron content in steel-making slag, J. Miner. Mater. Charact. Eng. 02 (2003) 65–70, https://doi.org/10.4236/jmmce.2003.21006.
[48] L. Jiang, Y. Bao, X. Hu, Y. Chen, G. Liu, F. Han, et al., Experimental investigation on BOF slag oxidation in air, Ironmak. Steelmak. 46 (2019) 747–754, https://doi.org/10.1080/03019233.2017.1410945.
[49] M. Choi, woo, Jung SM., Crystallization behavior of melted BOF slag during non-isothermal constant cooling process, J. Non-Cryst. Solids 468 (2017) 105–112, https://doi.org/10.1016/j.jnoncrysol.2017.04.042.
[50] Y. Satyoko, W.E. Lee, E. Parry, P. Richards, I.G. Houldsworth, Dissolution of iron oxide containing doloma in model basic oxygen furnace slag, Ironmak. Steelmak. 30 (2003) 203–208, https://doi.org/10.1179/030192303225003854.
[51] A. Niida, K. Okohira, A. Tanaka, T. Kai, Crystallization of free lime and magnesia from molten Ld-converter slag, Tetsu-To-Hagane/J. Iron Steel Inst. Japan 69 (1983) 42–50, https://doi.org/10.2355/tetsutohagane1955.69.1_42.
[52] H. Motz, J. Geiseler, Products of steel slags an opportunity to save natural resources, Waste Manag. 21 (2001) 285–293.
[53] P. Chaurand, J. Rose, J. Domas, J.Y. Bottero, Speciation of Cr and V within BOF steel slag reused in road constructions, J. Geochem. Explor. 88 (2006) 10–14, https://doi.org/10.1016/j.gexplo.2005.08.006.
[54] A.J. Hobson, D.I. Stewart, A.W. Bray, R.J.G. Mortimer, W.M. Mayes, M. Rogerson, et al., Mechanism of vanadium leaching during surface weathering of basic oxygen furnace steel slag blocks: a microfocus X-ray absorption spectroscopy and electron microscopy study, Environ. Sci. Technol. 51 (2017) 7823–7830, https://doi.org/10.1021/acs.est.7b00874.
[55] E. Schürmann, K.-H. Obst, L. Fiege, H.-P. Kaiser, Effect of bottom stirring and post stirring on the oxygen distribution between metal and slag at the end of the LD process, Steel Res. 56 (1985) 425–431, https://doi.org/10.1002/srin.198500660.
[56] G. Piñeiro, S. Perelman, J.P. Guerschman, J.M. Paruelo, How to evaluate models: observed vs. predicted or predicted vs. observed? Ecol. Model. 216 (2008) 316–322, https://doi.org/10.1016/j.ecolmodel.2008.05.006.
[57] J.M. Paruelo, E.G. Jobbágy, O.E. Sala, A.A. Okocha, W.K. Lauenroth, I.C. Burke, Functional and structural convergence of temperate grassland and shrubland ecosystems, Ecol. Appl. 8 (1998) 194–206, https://doi.org/10.1890/1051-0761(1998)008[0194:FASCOT]2.0.CO;2.
[58] H. Karimi, H.J.H. Brouwers, Accelerated thermal history analysis of light-burnt magnesium oxide by surface properties, Results Mater. 17 (2023), 100368, https://doi.org/10.1016/j.rinma.2023.100368.
[59] S. Ashrit, P.K. Banerjee, T.K. Ghosh, V. Rayasam, U.G. Nair, Characterisation of LD slag fines by X-ray diffraction, Metall. Res. Technol. 112 (2015) 1–9, https://doi.org/10.1051/metal/2015030.
[60] J.M. Park, Iron redox equilibria in BOF slag equilibrated with ambient air, Steel Res. 73 (2002) 39–43, https://doi.org/10.1002/srin.200200171.
[61] S. Wunderlich, T. Schirmer, U.E.A. Fittschen, Investigation on vanadium chemistry in basic-oxygen-furnace (BOF) slags—a first approach, Metals (Basel) 11 (2021) 1–15, https://doi.org/10.3390/met11111869.
[62] M.J. Ahmed, R. Cuijpers, K. Schollbach, S. Van der Laan, M. Van Wijngaarden-Kroft, T. Verhoeven, et al., V and Cr substitution in dicalcium silicate (C2s) under oxidizing and reducing conditions- synthesis, reactivity, and leaching behaviour studies, J. Hazard. Mater. 442 (2022), 130032, https://doi.org/10.2139/ssrn.4134122.
[63] J.C.O. Zepper, S.R. van der Laan, K. Schollbach, H.J.H. Brouwers, Reactivity of BOF slag under autoclaving conditions, Constr. Build. Mater. (2023) 364, https://doi.org/10.1016/j.conbuildmat.2022.129957.
[64] P. Stutzman, Direct Determination of Phases in Portland Cements by Quantitative X-ray Powder Diffraction, 2010.
[65] Standard Test Method for Determination of Proportion of Phases in Portland Cement and Portland-cement Clinker Using X-ray Powder, ASTM C1365-98, Annu. B. ASTM Stand, 2004, pp. 1–8.
[66] M.J. Fransen, A.C. Vermeulen, C13 1- and 2-dimensional detection systems and the problem of sample fluorescence in X-ray diffractometry, Powder Diffract. 18 (2003) 175, https://doi.org/10.1154/1.1706962.